Influence of sun zenith angle on canopy clumping and the resulting impacts on photosynthesis

Influence of sun zenith angle on canopy clumping and the resulting impacts on photosynthesis

Braghiere, Renato K.[1,2,3†], Quaife, Tristan[3,4], Black, Emily[3,5], Ryu, Youngryel[6], Chen, Qi[7], De Kauwe, Martin G.[8], Baldocchi, Dennis[9]

[1] Jet Propulsion Laboratory, California Institute of Technology, 4800 Oak Grove Drive, Pasadena, CA, 91109 USA

[2] Joint Institute for Regional Earth System Science and Engineering, University of California at Los Angeles, Los Angeles, CA, 90095 USA

[3] Department of Meteorology, University of Reading, UK

[4] National Centre for Earth Observation, University of Reading, Reading, UK

[5] National Centre for Atmospheric Science, University of Reading, Reading, UK

[6] Department of Landscape Architecture and Rural Systems Engineering, Seoul National University

[7] Department of Geography and Environment, University of Hawai'i at Mānoa, 435 Saunders Hall, 2424 Maile Way, Honolulu, HI 96822, USA

[8] Univ. of New South Wales, Sydney, NSW, Australia

[9] Department of Environmental Science, Policy, and Management, 137 Mulford Hall, University of California at Berkeley, Berkeley, CA 94720, USA

Corresponding author: Renato K. Braghiere (renato.braghiere@gmail.com)

†Current address: NASA Jet Propulsion Laboratory, M/S 233-305F, 4800 Oak Grove Drive, Pasadena, CA, 91109, USA.

Highlights

- Including angular variability in canopy structure improves 1D radiative transfer schemes
- The vertical distribution of light is impacted by angular variation in canopy structure
- Sites with dense vegetation are most impacted

Abstract

Addressing the impact of vegetation architecture on shortwave radiation transfer in land surface models is important for accurate weather forecasting, carbon budget estimates, and climate predictions. This paper investigates to what extent it is possible to retrieve structural parameters of two different parameterization schemes from direct transmittance derived from digital hemispherical photography and 3D radiative transfer modeling for two study sites with different vegetation canopy architectures. Neglecting the representation of 3D canopy structure in radiative transfer schemes leads to significant errors in shortwave radiation partitioning (up to 3.5 times more direct transmittance in the 3D model). Structural parameters, referred to as whole canopy 'clumping indices', were obtained in order to evaluate the impact of angular variation in clumping on shortwave radiation transfer. Impacts on photosynthesis were evaluated at site level with the UKESM land surface model, JULES. A comparison between flux tower derived and modeled photosynthesis indicates that considering zenith angular variations of structural parameters in the radiative transfer scheme of the UKESM land surface model significantly improves photosynthesis prediction in light limited ecosystems (from RMSE = 2.91 μmol $CO2.m^{-2}.s^{-1}$ to RMSE = 1.51 μmol $CO2.m^{-2}.s^{-1}$, 48% smaller), typically with enhanced photosynthesis from bottom layers.

Graphical abstract

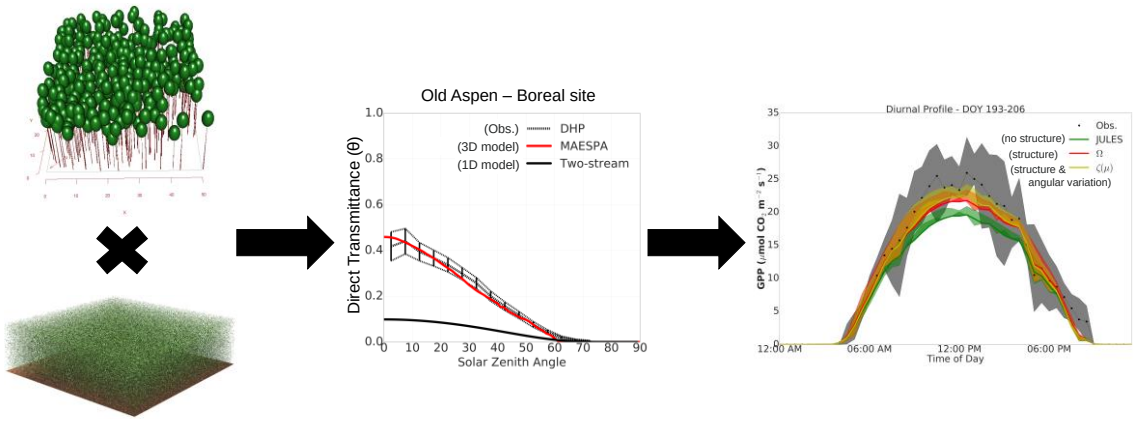

Keywords

Vegetation canopy architecture; vegetation structure; clumping index; Gross Primary Productivity; radiative transfer schemes; digital hemispherical photography; parameterization schemes

1. Introduction

Terrestrial ecosystems have been acting as a persistent carbon sink and absorbing almost a third of anthropogenic carbon emissions (Ciais et al., 2013; Le Quéré et al., 2018; Friedlingstein et al., 2019). Although a few observational studies (Keenan et al., 2016; Zhu et al., 2016; Chen et al., 2019) suggest the land surface benefits from elevated CO_2 concentration by 'greening', that does not necessarily translate into more carbon sequestration (Zhang et al., 2019), neither the persistence of the terrestrial carbon sink in the future is clear (Friedlingstein et al., 2006; Friedlingstein et al., 2014; Wieder et al., 2015). One route to addressing these open questions lies in improving Earth System Models (ESMs), which are fundamental tools for determining the future of climate and state of land ecosystems (Bonan and Deny, 2018).

One of the major factors leading to increased confidence in future climate predictions is the evolution of land surface models (LSMs), which have evolved to include realistic biological features linking photosynthesis and climate variables (Fung et al., 1983; Sellers, 1997; Pitman, 2003; Prentice et al., 2015). However, the way in which LSMs treat the transfer of radiation, water, and heat within vegetation and between the land and the atmosphere are still treated very simply (Ciais et al., 2013; Prentice et al., 2015).

LSMs necessarily make assumptions about the transfer of energy and mass between the land surface and the atmosphere in order to represent biological complexity into a tractable set of equations. These assumptions are often limited due to a lack of knowledge of all parameters involved in the calculations, lack of computational power to deal with such a level of detail over large areas for long periods of time, and incomplete theoretical descriptions for some processes related to biosphere-atmosphere exchanges (Loew et al., 2014). However, increased model complexity does not necessarily translate into reduced error (Prentice et al., 2015; Bonan and Doney, 2018).

The partitioning of solar radiation between various compartments of the land surface constitutes an important process to further quantify and understand the role of vegetation in distributing energy, which drives related biogeophysical processes, such as photosynthesis, evapotranspiration, changes in leaf and soil temperature, and snowmelt (Alton et al., 2007; Widlowski et al., 2011). The largest uncertainties in the global carbon cycle are due to the land carbon sink because of processes that are poorly represented or understood in LSMs (Le Quéré et al., 2018; Friedlingstein et al., 2019). Schaefer et al. (2012) evaluated daily average gross primary productivity (GPP) from 26 LSMs against estimated values at 39 eddy covariance flux tower sites across the United States and Canada and concluded that none of the LSMs match estimated GPP within observed uncertainty.

Canopy architecture may be thought of as the amount and organisation of aboveground plant material, which might include size, shape, orientation, and positional distribution of various plant organs (Norman and Campbell, 1989). Plant canopies can be structurally diverse due to unique spatial patterns that different species adopt for intercepting light and an even diversity of plant species which occupies a natural community (Atwell et al., 1999) and canopy architecture plays an important role in the partitioning of incident solar radiation, photosynthesis, transpiration, and momentum fluxes (Nilson, 1971; Goudriaan, 1977; Norman and Welles, 1983; Sellers, 1997; Pinty et al., 2006; Kobayashi et al., 2012; Loew et al., 2014; Dutta et al., 2017; Hogan et al., 2018; Braghiere et al., 2019).

The term canopy architecture is broad and not-limited to individual plants, while the level of complexity usually increases from uniform stands to heterogeneous plant communities. In this paper, vegetation canopy architecture is interpreted as the spatial separation of individual leaves or whole plants, i.e., ‘gaps’ in between and within the vegetation, with regions where shortwave radiation propagates without interacting with plant material.

Highly detailed canopy radiative transfer schemes (Wang and Jarvis, 1990; Ni et al., 1999; Gastellu-Etchegorry, 2008; Duursma and Medlyn, 2012) are too computationally expensive to be employed in large-scale studies over long-time periods (Song et al., 2009). However, some studies, such as that by Loew et al. (2014), have demonstrated that LSMs are likely to be significantly biased because they do not include descriptions of canopy architecture. To account for architectural effects of vegetation on shortwave radiation partitioning, some studies (Nilson, 1971; Baldocchi and Harley, 1995; Kucharik et al., 1999; Pinty et al., 2006; Ni-Meister et al., 2010) have attempted to develop efficient parameterization schemes in the radiative transfer schemes of LSMs by modulating the optical depth of the vegetation canopy through the addition of an effective variable so-called ‘clumping index’ (Nilson, 1971). The clumping

index defines the spatial distribution of leaves and trees (Norman and Jarvis, 1974), and it can be quantified based on gap size distribution measured by instruments like ceptometers (Leblanc et al., 2002; Ryu et al., 2010a) or DHPs (Chen and Cihlar, 1995; Leblanc et al., 2005). The clumping index was initially introduced as a constant value, but some studies (Pinty et al., 2006; Chen et al., 2008; Ryu et al., 2010; Ni-Meister et al., 2010) have proposed a sun zenith angle dependence on the clumping index.

Previous studies (Chen, 1996; Kucharik et al., 1999) reported that clumping index increases with sun zenith angle. However, Ryu et al. (2010) found the opposite behaviour of clumping index with sun zenith angle when analysing data collected in a discontinuous, open canopy blue oak woody savannah in California. The authors suggested that the radiation path length through a woody savannah decreases with sun zenith angle because the vegetation canopy is vertically elongated and horizontally dense. Large gaps are decomposed into smaller ones when the radiation path length is longer, which is a similar case to a random gap size distribution. The angular dependence of the clumping index was controlled by tree distribution at ecosystem scale over a heterogeneous woody savannah ecosystem and that might be a unique characteristic specific to this type of ecosystems.

This study seeks to understand the importance of considering sun zenith variation of clumping in a radiative transfer scheme of a LSM, particularly for carbon assimilation. The key driving question of this study is related to the possibility to retrieve a clumping indices that varies with sun zenith angle from digital hemispherical photographs (DHPs) derived direct transmittance. The focus of the analyses is based on two analytical parameterizations schemes: ‘the clumping index’ (Nilson, 1971) and ‘the structure factor’ (Pinty et al., 2006). A statistical evaluation of both parameterization schemes against observed data was perform for two flux-tower sites with distinct vegetation canopy architectures.

2. Methods and data

First, we explore observational methods to derive vegetation structural parameters using different treatments of DHPs to estimate the direct transmittance for two study sites. Second, we compare the values obtained through observations with results from a 3D land surface model, MAESPA (Duursma and Medlyn, 2012; Vezy et al., 2018) where structural LiDAR and dendrometry data were available. Third, we compare the direct transmittance derived from DHPs with the fitted direct transmittance for two different 'clumping indices', in order to determine whether the dependency of vegetation canopy architecture on zenith angle matters for the correct determination of the impact of canopy structural variability on shortwave radiation partitioning and carbon fluxes at site level.

2.1 The two-stream scheme and the JULES land surface model

The Joint UK Land Environment Simulator (JULES; Best et al., 2011; Clark et al., 2011) is the land surface model of the UK Earth System Model (UKESM), and it calculates light propagation and interaction with vegetation canopies by making use of a two-stream radiative transfer scheme (Sellers, 1985). The original version of the two-stream scheme was modified to include differences between sunlit and shaded leaves (Dai et al., 2004), sunfleck penetration (Mercado et al., 2007), and a clumping index (Williams et al., 2017).

In Dai et al. (2004), a one-layered, two-big-leaf submodel for photosynthesis, stomatal conductance, leaf temperature, and energy fluxes includes an improved two stream approximation model of radiation transfer of the canopy. The model separates integrations of radiation absorption by sunlit and shaded fractions of canopy, as well as a method for simultaneous solution of temperatures of the sunlit and shaded leaves. The model was later incorporated into the Common Land Model (CLM) with the simulated fluxes showing

improved agreement with the observations for the test cases of tropical evergreen broadleaf land cover and coniferous boreal forest.

In Mercado et al. (2007), a leaf-to-canopy scaling was added to JULES making explicit calculations at different levels in the vegetation canopy with the emphasis on a more realistic representation of light interception vertically (10 layers), and a defined foliar nitrogen value assuming an exponential decay, (and thus, the V_{cmax} parameter) at each canopy vertical level. Overall, the updated light interception formulation improved modeled photosynthesis when compared to a big leaf approach used in the original JULES formulation.

In here, the radiative transfer scheme in JULES was expanded to include the structure factor varying with zenith angle.

The concept of using the clumping index (Ω) (Nilson, 1971) in radiative transfer schemes to scale leaf area index (LAI) to account for heterogeneous canopy architecture has been commonly used in the literature (Kucharik et al., 1999; Pinty et al., 2006; Ni-Meister et al., 2010; Braghiere et al., 2019). This can be directly implemented into the two-stream scheme by using the effective LAI (LAI· Ω) instead of true LAI. Hence, the two stream equations following Sellers (1985) become:

$$\overline{\mu}\frac{(dI^{\uparrow})}{dLAI} + [1-(1-\beta)\omega]I^{\uparrow} - \omega\beta I^{\downarrow} = \omega\overline{\mu}\beta_0 \exp(-KL\cdot\Omega),$$

$$\overline{\mu}\frac{(dI^{\downarrow})}{dLAI} + [1-(1-\beta)\omega]I^{\downarrow} - \omega\beta I^{\uparrow} = \omega\overline{\mu}(1-\beta_0) \exp(-KL\cdot\Omega) \quad (1.0)$$

where $I^{\uparrow}$ and $I^{\downarrow}$ are the upward and downward diffuse radiative fluxes normalized by the incident flux at the top of the canopy; μ is the cosine of the Sun zenith angle, or the incident beam, K is the optical depth of direct beam per unit leaf area and is equal to G(μ)/μ, where G(μ) is the projected area of leaf elements in the direction $\cos^{-1}\mu$ (Ross, 1981), $\bar{\mu}$ is the average inverse diffuse optical depth per unit leaf area, ω is the scattering coefficient and is

given by $\rho_{leaf} + \tau_{leaf}$, the leaf reflectance and transmittance respectively, and L is the cumulative LAI from the top of the canopy. β and β_0 are upscattering parameters for the diffuse and direct beams, respectively.

The multilayer canopy is represented by increments of dLAI, which is equal to LAI divided by the number of layers. The of numbers of layers is flexible in the two-stream scheme, and it can be extended to any number greater than 1.

In the Eq. (1.0), Ω corresponds to: i) the clumping index (Nilson, 1971), or ii) the structure factor described in Pinty et al. (2006) assumed to vary with zenith angle.

The clumping index, or the structure factor, was introduced into the two-stream scheme by modifying three main groups of variables to account for canopy structural effects: i) the optical depth of direct beam per unit leaf area, K; ii) the average inverse diffuse optical depth per unit leaf area, $\bar{\mu}$, and; iii) the single scattering albedo, $\alpha_s(\mu)$, used to obtain the upscattering parameters for the diffuse and direct beams. For a detailed mathematical description of the equations modified in JULES, see appendix A.

After computing light interception, JULES calculates potential leaf-level photosynthesis as the minimum rate of three assimilation regimes as proposed by Farquhar et al. (1980) and modified by Collatz et al. (1991, 1992). Photosynthesis is calculated throughout a vertical multilayer vegetation canopy with 10 layers. As a direct result of the multilayered canopy approach, light becomes the prevalent limiting factor of photosynthesis towards the bottom of the canopy (Clark et al., 2011). However, when vegetation structure is considered in the radiative transfer scheme in JULES, light limited rate of photosynthesis is directly impacted but not the Rubisco or export limited rates, because the maximum rate of carboxylation (V_{cmax}) is proportional to

leaf Nitrogen concentration, that decays exponentially from the top to the bottom of the canopy in JULES (see Braghiere et al., 2019 for more details).

In JULES water limitation can affect photosynthesis in two different ways: first, through atmospheric water demand; and second, through soil moisture availability. Stomata conductance is calculated as:

$$g_s = \frac{1.6A_n}{1-f_0\left(1-\frac{D}{D_{critic}}\right)}\frac{1}{C_s-\Gamma} \quad (2.0)$$

where A_n is the gross flux uptake for photosynthesis minus leaf dark respiration, D is the vapour pressure deficit, C_S is the CO_2 concentration outside the stomata, which is equal to the atmospheric CO_2, f_0 is a factor related to the internal versus external leaf CO_2 concentration, D_{critic} is the maximum specific humidity deficit, and Γ is the CO_2 compensation point.

Soil moisture stress is considered by multiplying the potential photosynthetic rate by the stress function β (Cox et al., 1998) calculated as a combination of four soil layers. See Best et al. (2011) and Clark et al. (2011) for further details.

2.2 Clumping index

In order to characterize the impact of canopy architecture of vegetation on the radiation regime, Nilson (1971) first introduced a variable called the clumping index (Ω) into the Beer's law, to describe plant canopy direct transmittance, or the gap fraction, $P_{gap}(\theta)$:

$$P_{gap}(\mu) = \exp\left(\frac{-G(\mu)\cdot LAI\cdot\Omega}{\mu}\right) \quad (3.0)$$

where μ is the cosine of the sun zenith angle (θ), LAI is the leaf area index, and $G(\mu)$ is the projection coefficient of unit foliage area on a plane perpendicular to the view direction (Ross, 1981).

When Ω = 1, there is no clumping and leaves are considered to be randomly distributed. When Ω < 1, direct transmittance is enhanced by clumping, which is usually the case in most clumped vegetation canopies. It is also possible to find cases in nature where Ω > 1, which means that direct transmittance decreases with clumping effects. The cases where Ω exceeds 1 are associated with vegetation canopies exhibiting a significant number of woody elements, which contribute to the interception of shortwave radiation (Pinty et al., 2006).

Some of the main difficulties in correctly determining and evaluating the clumping index in forests include the mathematical methods to derive the parameters from direct transmittance data, the range of view zenith angles in which the data were collected, and how clumping index may or may not vary with zenith angle depending on the evaluated site (Ryu et al., 2010b).

2.3 Structure factor

Pinty et al. (2004) developed a parameterization that modulates the optical depth of a 1D canopy in a such a way as to simulate the behavior of 3D radiative transfer schemes. This parameterization scheme, referred to as the 'structure factor', is analogous to the clumping index, but with an extra parameter that accounts for zenith angle variations of structure. Pinty et al. (2006) described the structure factor parameterization as a robust approach since it guarantees accurate simulations for all components of the radiative partitioning (absorptance, reflectance, and transmittance) and it does not require an explicit description and understanding of the complex phenomena arising from the presence of heterogeneous vegetation architecture. The structure factor is defined as:

$$\Omega(\theta) = \zeta(\mu) = a + b \cdot (1 - \mu) \quad (4.0)$$

a = ζ(μ = 1) is the parameter corresponding to an overhead sun, and b the parameter responsible for including the effects of different sun geometries. In this study, both parameters (*a* and *b*)

were found by the Nelder-Mead minimization method (Nelder and Mead, 1964), or 'downhill simplex', against observed or modeled data.

2.4 MAESPA

The MAESPA model (Wang and Jarvis, 1990; Medlyn, 2004; Medlyn et al., 2007; Duursma and Medlyn, 2012) represents a forest canopy as an array of tree crowns, with specified tree dimension and positioning. Radiation calculations are only performed for a set of target crowns, specified by the user to save time, or for all trees if wanted (Wang and Jarvis, 1990). The distribution of leaf area within the target crown can be specified per individual tree, or for the whole stand, as well as the leaf angle distribution.

The target tree crown is divided into grid points, and the penetrating radiation at each grid point is calculated for three separate wavebands (PAR, NIR, and TIR) based on shading within and between crowns, sun zenith and azimuth angles, and the fractions of direct and diffuse radiation. Direct, diffuse, and scattered radiation are considered separately. Radiation scattering is obtained following the methodology in Norman (1979) and the leaf area index of a single tree crown is assumed to be distributed randomly within the crown (Wang and Jarvis, 1990), although other distributions (e.g., beta distribution in the vertical only, or vertical and horizontal directions) can be specified by the user. At each grid point, leaves are separated into sunlit and shaded following the scheme described in Norman (1993).

The MAESPA model has been applied to several study sites with different plant species (e.g., *Picea sitchensis*, *Pinus radiata*, *Betula pendula*, *Pinus taeda*) by different authors (Wang and Jarvis, 1990; Mcmurtrie and Wang, 1993; Wang et al., 1998; Medlyn, 2004; Vezy et al., 2018) for the study of energy and carbon fluxes.

2.5 Study sites

Observations of direct transmittance of light through forest canopies were obtained for 2 study sites in the Northern hemisphere over two plant functional types (PFTs): Deciduous Broadleaf Forest (DBF) and Woody Savannah (WS), following the International Geosphere-Biosphere Programme (IGBP) classification (Loveland and Belward, 1997). Further details are provided in Table 1.0 and a detailed description of the study sites can be found in their respective referenced literature. These two specific sites were selected because they have detailed structural data available, as well representing distinct canopy architectures and LAI values.

2.5.1 Old Aspen

The Southern Study Area - Old Aspen (SSA-OA) of the Boreal Ecosystem-Atmosphere Study (BOREAS) (53.876° N, 104.645° W) contains mostly old aspen (*Populus tremuloides*) trees, with an average age of 60 years, average tree height of 21 meters, and tree density of 1068 ha^{-1}. The growing season for aspen extends between May and September (Hogg et al., 2013). Mean annual air temperature at SSA-OA for the period 1971–2000 was 0.4°C and mean annual cumulative precipitation 467 mm (Chasmer et al., 2011).

DHPs were acquired from July 20th to August 17th 1994, in Summer, at three heights (0.8, 1.5, and 2.5 m) in separate sample transects. All DHPs were acquired at 10 m intervals along a central axis. The location of hemispherical photograph sample sites was determined in relation to the main flux tower in a transect established from 10 to 150 m Southwest of the tower (see Fig. 1.a).

For SSA-OA, P_{gap} data were taken from the dataset ‘BOREAS TE-23 Canopy Architecture and Spectral Data from Hemispherical photos’ (Rich et al., 1999). More information about experimental design and software used for DHP post-processing can be found in Chen et al. (1997).

The 60 m x 50 m mapped plot was used to characterize part of the forested surrounding of the flux tower. Detailed measurement of the mapped plot includes: i) stand characteristics (tree location, density, and basal area); ii) DBH of all trees in the designed area; and iii) detailed geometric measures of a subset of trees (height and crown dimensions) (Rich and Fournier, 1999). For any missing values the average value was considered.

The structural representation of the old aspen forest canopy (trees are represented by green circles in Fig. 1.a) is a partial representation of the canopy, 70 m away from the flux tower (represented by a red triangle). The DHPs were acquired along a straight line from the flux tower crossing the mapped plot area, represented by red circles.

The surroundings follow same patterns of canopy architecture as the measured area represented in Fig 1a. The green dotted area is not in the immediate closer vicinity of the tower in order to describe an area with stronger signal in the flux tower footprint. For more details on experiment logistics please refer to Chen et al. (1997).

2.5.2 Blue Oak

The Tonzi Ranch site (US-Ton) is classified as an oak-grass woodland savannah located in the lower foothills of the Sierra Nevada Mountains, California, USA (38.432° N, 120.967° W) at 177 m altitude on a terrain, under a Mediterranean-type climate with hot, dry summers and mild, rainy winters. This woody savannah site is dominated by blue oak trees (*Quercus douglasii*) with occasional (less than 10%) grey pine trees (*Pinus sabiniana*), and understory mainly composed of grasses (*Brachypodium distachyon*, *Hypochaeris glabra*) (Baldocchi et al., 2004). It presents a sparse vegetation cover of 47%, average tree density of 144 ha^{-1}, with average tree height at 9.4 ± 4.3 m, where trunk height is 1.8 ± 1.3 m, diameter at breast height (DBH) is 0.26 ± 0.11 m, and the average tree crown radius is 2.9 ± 1.4 m (Chen et al., 2008).

313 The site has been part of FLUXNET and AmeriFlux (http://public.ornl.gov/ameriflux/) since
314 2001. Further information can be found in other studies (Baldocchi et al., 2004; Ma et al., 2007;
315 Chen et al., 2008; Ma et al., 2016).

316 DHPs were acquired from 5th to 7th August 2008, close to the peak of the growing season, on
317 a 300 m x 300 m sampling plot with the flux tower at the center, gridded at 30 m x 30 m
318 intervals (Ryu et al., 2010). The extent of the plot corresponds to the scale of spatial
319 heterogeneity as determined through semivariogram analysis performed by Kim et al. (2006).

320 Figure 1.0b shows a representation of the mapped plot, where green circles represent the tree
321 trunk centers and red circles represent the places where the DHPs were acquired. The flux
322 tower is represented by the red triangle in the center of the plot.

323 **2.6 Data collection and pre-processing**

324 Direct transmittance for the blue oak site was extracted from the DHPs using the CIMES-
325 FISHEYE software (Walter, 2012) and were automatically thresholded via the Otsu method
326 (Otsu, 1979), where the images were reduced from grey level to a binary image. This method
327 assumes that the image contains two classes of pixels following a bi-modal histogram, i.e.,
328 foreground pixels representing the vegetation and background pixels representing the sky. It
329 then calculates the optimum threshold separating the two classes.

330 The binary form of the images was then divided into 5° zenith intervals, from 0° to 90° giving
331 a total of 18 equally divided intervals. The azimuth angles were also divided into 18 azimuthal
332 segments of 20° each. The last 3 points of the zenith profile were excluded from the statistical
333 analysis due to large uncertainty, hence a total of 15 points were used to represent the zenith
334 profile of direct transmittance from 0 to 75 degrees.

For the SSA-OA site, DHPs were digitized at a resolution of 512 (horizontal) × 480 (vertical) × 7 bits using the hemispherical photograph software CANOPY (Rich, 1989, 1990) archived in Kodak Photo CD format (Chen et al., 1997). The zenith profile of direct transmittance was obtained at 5° zenith angle intervals and separated into five zenith angles from 0° to 75° in order to compare the results obtained with hemispherical photographs and the ones obtained with LAI-2000. The LAI was calculated using the program LAICALC (Rich et al., 1995) following the method of Chen and Black (1991).

2.7 Modeling experiments

For the two study sites, the two-stream scheme in JULES v4.6 was modified to include the clumping index and the structure factor. The full model JULES v4.6 was then parameterized with observed meteorological and leaf spectral data. For the old aspen site, leaf reflectance in the PAR (400-700 nm) and NIR (780-2500 nm) spectral regions were averaged from the 'TE-08 spectral leaf' database (Spencer and Rock, 1999) with 1.66 nm spectral resolution, while a single averaged waveband soil albedo was taken from Betts and Ball (1997). The spectral data for the blue oak savannah is described in Kobayashi et al. (2012). Both sites were prescribed as broadleaf tree forests (one of the five plant functional types available in JULES). Leaf transmittance was calculated from the look-up table values of leaf scattering coefficient in the PAR and NIR wavebands. Spectral leaf properties are given in JULES for all leaves independent of their illumination characteristics, i.e., sunlit or shaded.

The model was run with the Global Land (GL) 4.0 configuration (Walters et al., 2014) for both sites in two distinct periods: i) for the old aspen site the model was run for a period of 13 days, from 11 to 24 July 1996. This period was selected based on meteorological and GPP data availability. The model was spun-up with yearly recycled meteorological data forcing for 5 years in order to determine initial steady states.

The DHPs were taken during Summer 1994, while the models were evaluated during Summer 1996. Vegetation canopy architecture does not change substantially in two years, unless some extraordinary event happens (e.g., fire, extreme winds, or land use change), and so, it was assumed that the old aspen canopy architecture remained unchanged between Summer 1994 and 1996. Also, the relatively short period of analysis was preferred in order to keep consistency within sun zenith angular variability and meteorological drivers; ii) for the blue oak savannah the model runs were performed from 1 to 14 August 2008, and the DHPs were acquired on 6 and 7 August 2008.

The meteorological and flux data were downloaded from the AMERIFLUX webpage (http://ameriflux.lbl.gov, accessed: August, 20th 2019), and the variables used to drive the model were: shortwave incident radiation, longwave incident radiation, liquid and frozen precipitation, surface temperature at 2 m, wind speed at 10 m, surface pressure, specific moisture, and incident diffuse shortwave radiation. The canopy radiation transfer was calculated by JULES using the multilayer two-stream scheme with the addition of sunfleck penetration following Dai et al. (2004) and implemented by Mercado et al. (2007) (can_rad_mod = 5 in JULES).

For the blue oak site, the diffuse radiation was measured directly and obtained from the Vaira ranch, which is about 2 km away from the flux tower in Tonzi ranch. For the old aspen site, the diffuse radiation was estimated through an empirical formula presented in Erbs et al. (1982), modified and validated by Black et al. (1991). The most important factor for shortwave radiation partitioning is the ratio between the total shortwave irradiance at the top of canopy, the sun zenith angle, and the solar constant (1360 W.m^{-2}). This formula was derived based on data obtained in the same latitudinal band near Vancouver, Canada, and therefore it is assumed to be applicable to the old aspen study site. The hydraulic soil characteristics for both sites were

383 also prescribed in the models based on observations. The LAI was prescribed as the same one
384 used for obtaining the structural parameters.

385 Five separate runs were performed with JULES for both study sites following different model
386 setups according to each one of the cases described in Table 3.0. The differences in GPP
387 between the modified JULES with both parameterization schemes and the non-clumped
388 version were summed over the vertical canopy across 10 layers and throughout the entire sun
389 zenith angular interval (from 0° to 90° in intervals of 6°) for each study site.

390 Finally, the MAESPA model was parameterized with: i) individual plants specified with
391 spatially explicit coordinates (see Fig 1a and Fig 1b); ii) the stand structure information,
392 including crown shape ('ellipsoid' for the old aspen site and 'half-ellipsoid' for the blue oak
393 site), spherical leaf incidence angle, uniform leaf area density, and variables related to decline
394 in wind speed with depth in the canopy and allometric relationships for biomass; iii) leaf
395 physiology model parameters, including spectral properties of leaves; and, iv) meteorological
396 observations to drive the model calculations.

397 The MAESPA model was used to calculate direct transmittance (Fig. 1e and Fig. 1f) and
398 fAPAR (Fig. 3a and Fig 3b) for both study sites. In order to obtain the direct transmittance
399 from MAESPA the leaf reflectance, leaf transmittance, and soil albedo were set to zero. P_{gap} is
400 calculated as 1 - fAPAR. In Figure 1.0e and Figure 1.0f the red lines represent P_{gap} from
401 MAESPA and the dashed black lines represent the P_{gap} derived from DHPs.

402 **2.8 Quantifying fitting performance of parameters derived from Digital Hemispherical**
403 **Photographs**

404 We derive the relevant parameters for both parameterization schemes, i.e., the clumping index
405 (Ω) from Nilson (1971) and both parameters (*a* and *b*) for the structure factor ($\zeta(\mu)$) from Pinty

et al. (2006), by inverting the adapted Beer's law equation (Eq. 3.0) against direct transmittance obtained from DHPs for two study sites in order to answer the question of whether or not the inclusion of a zenith-dependent structural parameterization presents a better agreement between the modeled and the observed data of gap probability derived from DHPs.

The leaf orientation function is derived using solid angle geometry (Ross, 1981; Myneni et al., 1989; Wang et al., 2007) and a commonly used assumption is that foliage angular distribution is random, or often referred to as 'spherical'. We assume a random leaf angle distribution with $G(\mu) = 0.5$, which is usually assigned to describe the projection coefficient for objects of any shape (Chen et al., 1997).

In order to quantify the performance of each one of the different parameterization schemes in fitting the observations, we make use of the Pearson correlation coefficient (r) and the root-mean-square-error (RMSE). Adding to our evaluation and in order to characterize whether the results arise due to model overfitting or not, we calculate two information criteria statistics, the Akaike information criterion (AIC; Akaike (1973)) and the Bayesian information criterion (BIC; Schwarz (1978)). According to Aho et al. (2014) these two indices were the two most popular measures of models' parsimony for ecological publications from 1993 to 2013.

4. Results

4.1 Comparison between modeled and measured direct transmittance

The calculated direct transmittance from DHPs is compared with the one calculated by the MAESPA model and the one calculated with the two-stream scheme for the old aspen site and the blue oak, two substantially different study sites in term of canopy architecture and LAI.

The direct transmittance derived from DHPs and the one modeled by MAESPA are within the 95% confidence interval for both sites (Fig. 1e and Fig 1f.). For the old aspen site especially, until about 20 degrees the modeled P_{gap} is very close to the mean, while for the other part of the curve the calculated P_{gap} underestimates the mean but is within the lower limit of the 95% confidence interval. The old aspen forest has a high LAI (LAI = 4.63 $m^2.m^{-2}$) and it is a dense area with 356 trees in a 50 m x 60 m area plot, which results in P_{gap} going to zero at about 60 degrees zenith angle.

The results from the unmodified two-stream scheme underestimate both curves by up to 0.30 in P_{gap} at zero degrees zenith angle, and it is not able to reproduce the shape of the other curves either. This implies its usage can lead to discrepancies in fAPAR and albedo estimates as well. The blue oak site is a much sparser canopy with 604 trees in a 300 x 300 m^2 area with lower LAI (LAI = 0.70 $m^2.m^{-2}$) but the agreement between the calculated P_{gap} and the one derived from observations is still close. For this study site the two-stream scheme also underestimates the direct transmittance but not as much as for the old aspen site. The underestimation of P_{gap} by the two-stream scheme is in the order of 0.10 for zero degrees sun zenith angle. The shapes of direct transmittance curves as a function of zenith angle are similar between MAESPA and DHPs until about 80 degrees but after that MAESPA underestimates the values obtained through DHPs.

At high zenith angles the spread between the P_{gap} curves in the blue oak site is quite significant and even though the MAESPA model disagrees with the observation, only values up to 75 degrees are considered in the statistical analysis. P_{gap} curves converge at high zenith angles for the old aspen site, while that is not observed for the blue oak site. It is also important to highlight that the canopy representation in MAESPA is finite and limited to the size of the plotted area, while in nature the forest canopy extends over a much larger area.

Based on these evaluations over two sites with distinct values of LAI it is possible to provide an accurate value of direct transmittance from 3D radiative transfer modeling from the MAESPA model parameterized with different types of structural data, i.e., manual dendrometry measurements and/or LiDAR data.

4.2 Deriving clumping indices from observed data

Table 2.0 summarizes the fitting performance to observed data of both parameterization schemes for both study sites. The RMSE associated with the fit of the clumping index is always larger than the RMSE associated with the fit of the structure factor, which indicates that varying clumping with sun zenith angle gives a better description of direct transmittance throughout the day than having a fixed single value of clumping. Both AIC and BIC obtained for the structure factor fit are smaller than the ones obtained for the clumping index for both evaluated cases, indicating that the better fit of the structure factor is not due to the increased number of free parameters compared to the clumping index.

4.3 The impact of structural parameterizations on GPP at site level

JULES v4.6 was run for the same amount of time (13 days) for both study sites with three different experimental set ups: i) the default two-stream scheme (JULES), ii) the parameterized version of two-stream scheme with clumping index (Ω), and iii) with the structure factor ($\zeta(\mu)$). The resulting fAPAR curves are shown in Figure 3.0a and Figure 3.0b and GPP curves are presented in Figure 3.0c and Figure 3.0d. The fAPAR curves are not smooth because of the presence of variable amounts of diffuse radiation.

For the old aspen site, the differences in fAPAR are limited to 0.15 or less, especially when associated with lower sun zenith angles, i.e., for the beginning and end of the solar day. Both fAPAR curves calculated with the parameterized two-stream present a lower fAPAR than the

default version of the two-stream scheme. It is also important to note that the fAPAR obtained through the two-stream scheme with the structure factor parameterization is the lowest at 12 noon local time. The middle of the day is associated with small values of sun zenith angle, and the path length through the canopy is shorter for small sun zenith angles. Towards sunrise and sunset the structure factor is larger because the sun zenith angle is higher, and the b parameter is positive in this site, i.e., b = 0.627.

For the blue oak site, the difference between the default two-stream and the parameterized versions is significant (up to 0.20) because LAI is relatively small (LAI = 0.70 $m^2.m^{-2}$). Impacts on fAPAR calculations via the two-stream scheme are more significant for smaller values of LAI, because the amount of absorbed radiation grows exponentially with LAI towards saturation. For the blue oak site, the structure factor has a small negative value of *b* (b = -0.097), and the term *a* of the structure factor and the clumping index are within the same confidence interval, i.e., a = 0.492(0.447,0.537) and Ω = 0.462(0.434,0.490). Ryu et al. (2010) determined a spatially representative clumping index of 0.490 for the blue oak site, which is compatible with the value found in our study. The differences in fAPAR calculated with the two-stream parameterized with clumping index and the one parameterized with structure factor are negligible. Both curves agree with fAPAR from MAESPA for most of the day.

Although the fAPAR obtained for the old aspen site with the two-stream scheme parameterized with the structure factor was the smallest, the GPP obtained through this scheme was the largest. Both structural parameterization schemes act to increasd the model's light use efficiency (LUE) , because this site has a relatively high value of LAI and hence bottom layers of the old aspen site are mostly light limited through the day (Fig. 5.0a) Taking vegetation architecture into account when calculating shortwave radiative transfer allows more shortwave

497 radiation to reach further layers at the bottom of the vegetation canopy, which alleviates light
498 limitation for those layers.

499 The comparison between flux tower and modeled GPP indicates that considering architectural
500 heterogeneity on the radiative transfer scheme in JULES improves the model predictions for
501 the evaluated period in the old aspen site. The results are confirmed by the RMSE values
502 improve from 2.91 $\mu mol.CO_2.m^{-2}.s^{-1}$ for the default two-stream scheme in JULES v4.6 to 1.75
503 $\mu mol.CO_2.m^{-2}.s^{-1}$ when the clumping index parameterization scheme is applied, and 1.51
504 $\mu mol.CO_2.m^{-2}.s^{-1}$ when the structure factor parameterization scheme is used. The boreal site is
505 located at a high Northern latitude (53.629° N) with bottom layers of the vegetation mostly
506 limited by light according in the Farquhar model.

507 For the blue oak site, there are three key findings: first, in the early morning (06:00 AM to
508 09:00 AM local time) the agreement between the flux tower and modeled GPP within all
509 experimental set ups is relatively high, and even though the difference in fAPAR between the
510 schemes is up to 0.20, the difference in calculated GPP is small; second, the blue oak site is a
511 savannah with considerable water limitation and from 09:00 AM to 03:00 PM the surface
512 temperature and vapor pressure deficit (VPD) increase substantially, which are conditions more
513 likely to result in a carbon limiting regime in the Farquhar model (Fig. 5.0b) because the trees
514 close their stomata and reduce total photosynthesis in order to avoid potential water losses.
515 Both flux tower and modeled GPP decrease during this period but the modeled GPP decreases
516 at a higher rate than the one derived from flux tower measurements. This highlights a potential
517 misrepresentation of the stomata response by JULES over a savannah site.

518 A possible explanation for a misrepresentation of the stomata response in JULES is related to
519 root depth being large in the blue oak site (Raz-Yaseef et al., 2013) and not correctly described
520 in the model. In order to isolate only the effects of changes in the radiative transfer scheme due

to horizontal heterogeneity in canopy architecture, no changes were made to other parts of the model, including rooting depth, to maintain the original JULES configuration as close as possible to the default case, i.e., JULES version 4.6 with the Global Land (GL) 4.0 configuration (Walters et al., 2014).

Third, GPP from the model responds positively to the decay of temperature and VPD, with an increase at the very end of the solar day. However, this behavior is not observed in the flux tower GPP, which suggests a natural slow response on the stomatal opening. The blue oak in this site showed very large seasonal variations of V_{cmax}, from 30 to 150 μmol m^{-2} s^{-1} (Xu and Baldocchi, 2003). However, due to the short period of time evaluated (two first weeks of August 2008) V_{cmax} only varied due to temperature changes in the range from 20 to 40 μmol m^{-2} s^{-1}.

The RMSE values for the different model representations are roughly the same for this blue oak site (0.83 μmol.CO_2.m^{-2}.s^{-1}) and smaller than the ones presented for the old aspen site, mainly because the total flux tower GPP in the boreal site is five times larger than the GPP in the blue oak site; the same order of difference as in LAI.

4.4 Evaluating impacts of structural parameterizations on photosynthesis limiting regimes at site level

4.4.1 Isolating the factors affecting photosynthesis

In order to isolate the impact of canopy architecture on photosynthesis, the influence of five different factors were tested separately including: i) differences in the nature of light, i.e., whether incident radiation is in a diffuse or direct form; ii) soil albedo; iii) the spectral properties of the leaves; and, iv) the vertical profile of leaf nitrogen concentration, which affects values of V_{cmax} and, therefore, modifies carbon and transport limiting rates (see Clark

et al., 2011). The configuration of each case is shown in Table 3.0 and differences in GPP between the control run and both parameterization schemes are shown in Figure 4.0 with associated deviations indicated by black error bars.

The behavior in Case 1 can be explained by the presence of more productive bottom layers with higher nitrogen content receiving more shortwave radiation due to the consideration of canopy spatial heterogeneity. The summed difference of GPP throughout the vertical canopy over the whole sun zenith interval in the old aspen site is roughly 5 times larger than in the blue oak site because of much higher LAI values in the former site.

In case 2, leaf nitrogen concentration follows an exponential decay throughout the vertical axis towards the bottom. As a result, the most productive layers are located at the top of the canopy. Smaller differences in GPP in case 2 compared to case 1 relates to less productive bottom canopy layers, and so, the impact of structural parameterization schemes decrease.

In case 3, scattering processes reflect part of the shortwave radiation isotropically upwards and downwards, and because of the isotropic nature of diffuse light, there is a total reduction on the effect of canopy spatial heterogeneity on GPP enhancement. In general, heterogeneous architecture has a lower impact on GPP enhancement in the presence of isotropic radiation. This behavior can be seen in both sites represented in Figure 4.0.

In case 4, with the addition of a reflective soil underneath the vegetation canopy, the impacts of heterogenous architecture on JULES GPP behave differently in each study site. For the old aspen site in Canada, the difference in GPP increases when observed values of soil reflectance are used in JULES because part of the incident shortwave radiation in the soil is reflected upwards and has the possibility to interact with the vegetation canopy equally in all directions. In this case, canopy architecture interacts with the shortwave radiation going upwards from the

bottom of the canopy, and in the dense old aspen site the difference in GPP enhancement is larger when soil reflectance is considered. This behavior, however, is not observed in the blue oak site in California, because the latter is so sparse that radiation reflected upwards has only a small chance to interact with the canopy. Changing soil reflectance in a site with high LAI values results in greater sensitivity of GPP to the architecture of the canopy than in sites with low LAI values.

Finally, in case 5, the measured proportion of incident diffuse shortwave radiation is considered. It is possible to verify that for the old aspen site the difference in GPP between the homogeneous and the heterogeneous canopy architectures shows a slight decrease, while in the blue oak site, there is an inversion of sign of GPP difference, which means that adding a structural parameterization scheme has a negative impact on GPP. Most of the incident shortwave radiation was direct during the evaluated period in SSA-OA, which explains a small difference in GPP. In US-Ton, the sparse character of the site associated with a low LAI value results in a large part of the soil being exposed to shortwave radiation, and so, a large part of the radiation is reflected backwards leaving the canopy without being absorbed, which explains the reduction on photosynthetic rate. However, this is the only case in which GPP difference is negative.

4.4.2 The impact of structural parameterizations on photosynthesis limiting regimes

Vertical profiles of the Farquhar model limiting regimes were vertically derived from JULES for the two sites by calculating the potential photosynthesis in each one of the three limiting regimes, i.e., carbon (▲), light (●), and electron export (+), and selecting the regime with the minimum value as the limiting regime. Figure 5.0a shows the vertical zenith profile of GPP and the photosynthesis limiting regimes obtained from JULES v4.6. The vertical GPP values

590 and the vertical photosynthesis limiting regime were averaged through the day and are
591 presented in a zenith profile.

592 The most productive layers in the old aspen site are located at the top of the canopy for smaller
593 values of sun zenith angles, i.e., when there is more shortwave radiation available. The carbon
594 limiting regime is associated with higher values of GPP, and light limiting regime is associated
595 with smaller values of GPP for larger sun zenith angles and deeper layers of the canopy. There
596 is no evident dependence between GPP and sun zenith angle for the blue oak site in California,
597 although there can be more GPP in upper layers of the canopy related to higher nitrogen
598 concentration represented in JULES. Although there are no measured vertical leaf nitrogen
599 profiles available in the blue oak site, trees are quite exposed to abundant sunlight, and so, there
600 is not likely to be much vertical variation in the nitrogen content.

601 Accounting for vegetation canopy architecture through the addition of a structural
602 parameterization in the two-stream scheme in JULES had a major impact on the photosynthesis
603 limiting regime over the old aspen site throughout the canopy. The positive difference in GPP
604 comes mainly from the bottom layers, that are now limited by carbon instead of being limited
605 by light, and the positive difference in GPP is associated with smaller values of sun zenith
606 angle.

607 The structure factor parameterization scheme switches the photosynthesis limiting regimes of
608 the last four layers of the canopy for angles smaller than 40° for the old aspen site, while the
609 clumping index affects layers 7 to 9 but does not affect the very bottom layer. This change in
610 photosynthesis limiting regime can be perceived by a higher value of GPP obtained through
611 the structure factor parameterization scheme in the middle of the day (Fig. 3.0). The impacts
612 on GPP and limiting regimes for the blue oak site are negligible.

5. Discussion

Our goal in this paper was to evaluate the performance of two distinct parameterizations schemes in order to account for the impact of structural heterogenous vegetation canopies on the transfer of shortwave radiation and carbon assimilation. To do so, we modified a two-stream radiative transfer scheme commonly used in LSMs and we derived the required parameters from fieldwork observations of direct transmittance with DHPs for two study sites.

In a previous study, Bonan et al. (2011) indicated an inconsistency of radiation absorption calculated by a version of the two-stream scheme used in the Community Land Model (CLM) 4 (Sellers et al., 1996; Thornton and Zimmermann, 2007; Oleson et al., 2010). The authors showed that CLM4 was overly sensitive to diffuse radiation because of the theoretically incorrect diagnosis of sunlit and shaded leaf radiation, remarkably different from the analytical solution of Dai et al. (2004). The authors suggested CLM4 overestimates absorption of diffuse radiation by shaded leaves, which partly explains why CLM4 presented a high GPP bias, particularly in the tropics. In another study using JULES, Alton et al., (2007a,b) highlighted large differences (up to 25%) in GPP, especially in the tropics, predicted by two different ways of treating radiative transfer: beer's law and the two-stream scheme. The authors suggested that using a big leaf approximation leads to an overestimation of canopy LUE and an incapability to capture more radiation absorption under increased diffuse sunlight. These results are both linked to inaccurate representations structure in radiative transfer schemes.

In a more recent study with the Ecosystem Demography model (ED2), Viskari et al. (2019) indicated that uncertainty in model projection of Net Primary Production (NPP) depends on uncertainties in model parameters and canopy structure, particularly canopy clumping and leaf optical properties. The authors highlighted that larger changes in light profile within the vegetation canopy could be masked due to an 'apparent' reduced sensitivity of model response

637 to different parameterizations of the radiative transfer scheme, especially in structurally
638 complex vegetation. They also indicated that some light-starved parts of the vegetation canopy
639 predicted in their model were not aligned with observations.

640 Likewise, we found that the two-stream scheme underestimates direct transmittance due to
641 differences in canopy architecture independently of vegetation density We found that for both
642 study sites using a clumping index that varies with sun zenith angle produced a better
643 performance than a simple scalar clumping index.

644 Nonetheless, it is important to recognize potential sources of uncertainty arising from use of
645 these clumping schemes and the derivation of the associated parameters. First, there are
646 significant uncertainties in LAI due to the derivation method. Second, leaf spectral data and
647 incident diffuse radiation are also important variables required by the two-stream scheme, and
648 they are often not measured at site level. Third, the impacts of different leaf angle distributions
649 on radiation partitioning were not evaluated here, but may have a significant effect on the
650 radiation partitioning in vegetation canopies. A recent study has shown that global Solar
651 Induced Fluoresce is particularly sensitive to leaf angle distribution, but GPP seems to be
652 relatively insensitive to the leaf angle (Norton et al., 2019).

653 The overall effect of considering a vegetation clumping index that varies with sun zenith angle
654 were clear, but this effect differed between the characteristics of two sites, with VPD as an
655 important driver, as previously reported in other studies (Xu et al., 2003; Osuna et al., 2015).
656 The magnitude in GPP was more limited by incoming solar radiation at the boreal site in
657 summer, whereas, in the blue oak site, GPP was light-saturated, with maximum values
658 determined by a VPD threshold (Goodrich et al., 2015).

Water limited sites are mostly constrained by internal leaf carbon concentrations due to stomatal closure, therefore changes in the radiative transfer scheme are not as impacting on carbon assimilation as other factors could be, such as soil water content or VPD. The blue oak site is a good example of whether considering structural heterogeneity through a parameterization applied to the radiative transfer scheme could be highly impacting, mainly because it is a sparse woody savannah, and changes in fAPAR due to architecture are quite significant (Fig. 3.0b). However, including architectural heterogeneity when estimating GPP does not have The photosynthesis limiting regimes of a large impact because light is not the main limiting regime in the Farquhar model for this study site (Fig. 5.0b).

Although total canopy fAPAR is smaller when including canopy architecture in the two-stream scheme, it also allows more shortwave radiation to propagate into deeper layers in the forest canopy, increasing GPP by the model over sites where the bottom layers are light limited. The agreement between flux tower and modeled GPP improves with structural parameterizations in the radiative transfer scheme, independently of the direct or diffuse nature of incident light, soil albedo, leaf spectral properties, or vertical profile of leaf nitrogen concentration.

These parameterization schemes of canopy architecture are straightforward to be applied in LSMs and can be useful to improve GPP predictions in heterogenous forest canopies. The parameters required to drive the radiative transfer scheme can be derived from DHPs, ceptometers, as well as from 3D radiative transfer models, which can be useful for study sites with a limited number of vegetation canopy structural data.

6. Conclusion

This paper investigated the impacts of two different vegetation architecture parameterization schemes, applied to the Sellers two-stream radiative transfer model in JULES, and used parameters derived from fieldwork observations of direct transmittance with DHPs.

Through the modification of the two-stream scheme, canopy architecture allows more shortwave radiation to propagate into deeper layers in the forest canopy, increasing GPP by the model over sites where the bottom layers are light limited. The agreement between flux tower and modeled GPP improves.

A better agreement between modeled and flux tower GPP was only observed in a mostly light limited forest. This result was not observed on a carbon limited savannah site, and even though the impact of the structure factor on fAPAR was substantial, the actual impact on GPP was negligible. Photosynthesis limiting regimes in the old aspen boreal site changed when vegetation architecture was included.

The improvement on GPP predictions via land surface modeling was dependent on the characteristics of the vertical distribution of photosynthesis limiting regimes of each one of the evaluated sites, indicating that the variation of clumping index with sun zenith angle is more important over denser sites with higher LAI, and ultimately limited to locations where light limitation overcomes the other limiting regimes of the Farquhar model in LSMs.

Author Contributions

R. K. B. designed the study, modified JULES, conducted all the analyses, and wrote the manuscript. T.Q. implemented the parameterization scheme with zenith angular variations. T.Q. and E.B. coordinated the progress of the study and contributed to the writing of the manuscript. Y.R., M.G.D.K. collected and shared part of the DHPs. Q.C. and D.B. are

responsible for the collection, pre-processing, and sharing of LiDAR data collected at Tonzi Ranch, California. All authors helped improving the writing of the manuscript.

Conflict of interest

The authors declare to have no competing financial interests.

Acknowledgments

This work was conducted during a PhD scholarship supported by the 'Science without Borders' Program at the University of Reading (grant number 9549-13-7). Financed by CAPES – Brazilian Federal Agency for Support and Evaluation of Graduate Education within the Ministry of Education of Brazil. Tristan Quaife's contribution was funded by the NERC National Centre for Earth Observation. This research was carried out in part at the Jet Propulsion Laboratory, California Institute of Technology, under a contract with the National Aeronautics and Space Administration. California Institute of Technology. Government sponsorship acknowledged. Copyright 2020. All rights reserved. The authors would like to thank Pier-Luigi Vidale, Sue Grimmond, and Peter North for discussions on radiative transfer and carbon budget. A UNIX patch file for JULES version 4.6 is available from https://github.com/braghiere/JULES-Clump. The JULES code is available from the UK Met Office code repository: https://code.metoffice.gov.uk/. Model simulation results were made available with this publication. The authors thank three anonymous reviewers whose comments improved the manuscript.

References

Aho, K., Derryberry, D., Peterson, T., 2014. Model selection for ecologists: the worldviews of AIC and BIC. Ecology 95, 631–636. https://doi.org/10.1890/13-1452.1

724 Akaike, H., 1973. Information theory and an extension of the maximum likelihood principle,
725 in: Kaido, A. (Ed.), Second International Symposium on Information Theory. Budapest,
726 Hungary, pp. 267–281.
727 Alton, P.B., Ellis, R., Los, S.O., North, P.R., 2007. Improved global simulations of gross
728 primary product based on a separate and explicit treatment of diffuse and direct sunlight.
729 J. Geophys. Res. Atmos. 112, 1–12. https://doi.org/10.1029/2006JD008022
730 Alton, P., Mercado, L., North, P., 2007. A sensitivity analysis of the land-surface scheme
731 JULES conducted for three forest biomes: Biophysical parameters, model processes, and
732 meteorological driving data. Global Biogeochem. Cycles 21.
733 Atwell, B., Kriedemann, P., Turnbul, C., 1999. Plants in Action: Adaptation in Nature,
734 Performance in Cultivation, Plants in Action. Macmillan Education Australia.
735 Baldocchi, D.D., Harley, P.C., 1995. Scaling carbon dioxide and water vapour exchange from
736 leaf to canopy in a deciduous forest. II. Model testing and application. Plant, Cell Environ.
737 18, 1157–1173. https://doi.org/10.1111/j.1365-3040.1995.tb00626.x
738 Baldocchi, D.D., Xu, L., Kiang, N., 2004. How plant functional-type, weather, seasonal
739 drought, and soil physical properties alter water and energy fluxes of an oak-grass savanna
740 and an annual grassland. Agric. For. Meteorol. 123, 13–39.
741 https://doi.org/10.1016/j.agrformet.2003.11.006
742 Baldocchi, D., 2006. Measuring and Modeling Carbon, Water Vapor and Energy Exchange
743 over Grassland and Tree/Grass Ecosystems. Berkeley, California, USA.
744 Best, M.J., Pryor, M., Clark, D.B., Rooney, G.G., Essery, R.L.H., Menard, C.B., Edwards,
745 J.M., Hendry, M. a., Porson, a., Gedney, N., Mercado, L.M., Sitch, S., Blyth, E., Boucher,
746 O., Cox, P.M., Grimmond, C.S.B., Harding, R.J., 2011. The Joint UK Land Environment
747 Simulator (JULES), model description. Part 1: Energy and water fluxes. Geosci. Model
748 Dev. 4, 677–699.

749 Betts, A.K., Ball, J.H., 1997. Albedo over the boreal forest. J. Geophys. Res. Atmos. 102,
750 28901–28909. https://doi.org/10.1029/96JD03876
751 Black, T.A., Chen, J.-M., Lee, X., Sagar, R.M., 1991. Characteristics of shortwave and
752 longwave irradiances under a Douglas-fir forest stand. Can. J. For. Res.
753 https://doi.org/10.1139/x91-140
754 Bonan, G.B., Doney, S.C., 2018. Climate, ecosystems, and planetary futures: The challenge to
755 predict life in Earth system models. Science (80-.). 359, eaam8328.
756 https://doi.org/10.1126/science.aam8328
757 Braghiere, R.K., Quaife, T., Black, E., He, L., Chen, J.M., 2019. Underestimation of Global
758 Photosynthesis in Earth System Models Due to Representation of Vegetation Structure.
759 Global Biogeochem. Cycles 2018GB006135. https://doi.org/10.1029/2018GB006135
760 Campbell, G.S., Norman, J.M., 1989. The description and measurement of plant canopy
761 structure, in: G, R., B, M., PG, J. (Eds.), Plant Canopies: Their Growth, Form and
762 Function. Cambridge University Press, Cambridge, pp. 1–19.
763 Chasmer, L., Kljun, N., Hopkinson, C., Brown, S., Milne, T., Giroux, K., Barr, A., Devito, K.,
764 Creed, I., Petrone, R., 2011. Characterizing vegetation structural and topographic
765 characteristics sampled by eddy covariance within two mature aspen stands using lidar
766 and a flux footprint model: Scaling to MODIS. J. Geophys. Res. 116, G02026.
767 https://doi.org/10.1029/2010JG001567
768 Chen, C., Park, T., Wang, X., Piao, S., Xu, B., Chaturvedi, R.K., Fuchs, R., Brovkin, V., Ciais,
769 P., Fensholt, R., Tømmervik, H., Bala, G., Zhu, Z., Nemani, R.R., Myneni, R.B., 2019.
770 China and India lead in greening of the world through land-use management. Nat. Sustain.
771 2, 122–129. https://doi.org/10.1038/s41893-019-0220-7
772 Chen, J.M., Cihlar, J., 1995. Plant canopy gap-size analysis theory for improving optical
773 measurements of leaf-area index. Appl. Opt. 34, 6211–6222.

774 Chen, J.M., 1996. Optically-based methods for measuring seasonal variation of leaf area index
775 in boreal conifer stands. Agric. For. Meteorol. 80, 135–163. https://doi.org/10.1016/0168-
776 1923(95)02291-0
777 Chen, J.M., Black, T.A., 1991. Measuring leaf area index of plant canopies with branch
778 architecture. Agric. For. Meteorol. https://doi.org/10.1016/0168-1923(91)90074-Z
779 Chen, J., Rich, P., 1997. Leaf area index of boreal forests: Theory, techniques, and
780 measurements. J. Geophys. Res. 102, 29429. https://doi.org/10.1029/97JD01107
781 Chen, Q., Baldocchi, D., Gong, P., Dawson, T., 2008. Modeling radiation and photosynthesis
782 of a heterogeneous savanna woodland landscape with a hierarchy of model complexities.
783 Agric. For. Meteorol. 148, 1005–1020.
784 Ciais, P., Sabine, C., Bala, G., Bopp, L., Brovkin, V., Canadell, J., Chhabra, a, DeFries, R.,
785 Galloway, J., Heimann, M., Jones, C., Quéré, C. Le, Myneni, R.B., Piao, S., Thornton, P.,
786 2013. Carbon and Other Biogeochemical Cycles. Clim. Chang. 2013 - Phys. Sci. Basis.
787 https://doi.org/10.1017/CBO9781107415324.015
788 Clark, D.B., Mercado, L.M., Sitch, S., Jones, C.D., Gedney, N., Best, M.J., Pryor, M., Rooney,
789 G.G., Essery, R.L.H., Blyth, E., Harding, R.J., Hutingford, C., Cox, P.M., 2011. The Joint
790 UK Land Environment Simulator (JULES), model description. Part 2: Carbon fluxes and
791 vegetation dynamics. Geosci. Model Dev. 4, 701–722. https://doi.org/10.5194/gmd-4-
792 701-2011
793 Collatz, G.J., Ribas-Carbo, M., Berry, J. a., 1992. Coupled photosynthesis-stomatal
794 conductance model for leaves of C4 plants. Aust. J. Plant Physiol. 19, 519–539.
795 https://doi.org/10.1071/PP9920519
796 Collatz, G.J., Ball, J.T., Grivet, C., Berry, J. a, 1991. Physiological and environmental
797 regulation of stomatal conductance, photosynthesis and transpiration: a model that

includes a laminar boundary layer. Agric. For. Meteorol. 54, 107–136. https://doi.org/10.1016/0168-1923(91)90002-8

Dai, Y., Dickinson, R., Wang, Y., 2004. A Two-Big-Leaf Model for Canopy Temperature , Photosynthesis , and Stomatal Conductance. J. Clim. 17, 2281–2299. https://doi.org/10.1175/1520-0442(2004)017<2281:ATMFCT>2.0.CO;2

Dutta, D., Wang, K., Lee, E., Goodwell, A., Woo, D.K., Wagner, D., Kumar, P., 2017. Characterizing Vegetation Canopy Structure Using Airborne Remote Sensing Data. IEEE Trans. Geosci. Remote Sens. 55, 1160–1178. https://doi.org/10.1109/TGRS.2016.2620478

Duursma, R.A., Medlyn, B.E., 2012. MAESPA: A model to study interactions between water limitation, environmental drivers and vegetation function at tree and stand levels, with an example application to [CO2] x drought interactions. Geosci. Model Dev. 5, 919–940.

Erbs, D.G., Klein, S.A., Duffie, J.A., 1982. Estimation of the diffuse radiation fraction for hourly, daily and monthly-average global radiation. Sol. Energy 28, 293–302.

Farquhar, G.D., Caemmerer, S., Berry, J.A., 1980. A biochemical model of photosynthetic CO2 assimilation in leaves of C3 species. Planta 149, 78–90. https://doi.org/10.1007/BF00386231

Friedlingstein, P., Cox, P., Betts, R., Bopp, L., von Bloh, W., Brovkin, V., Cadule, P., Doney, S., Eby, M., Fung, I., Bala, G., John, J., Jones, C., Joos, F., Kato, T., Kawamiya, M., Knorr, W., Lindsay, K., Matthews, H.D., Raddatz, T., Rayner, P., Reick, C., Roeckner, E., Schnitzler, K.G., Schnur, R., Strassmann, K., Weaver, A.J., Yoshikawa, C., Zeng, N., 2006. Climate-carbon cycle feedback analysis: Results from the C4MIP model intercomparison. J. Clim. https://doi.org/10.1175/JCLI3800.1

Friedlingstein, P., Meinshausen, M., Arora, V.K., Jones, C.D., Anav, A., Liddicoat, S.K., Knutti, R., 2014. Uncertainties in CMIP5 Climate Projections due to Carbon Cycle Feedbacks. J. Clim. 27, 511–526. https://doi.org/10.1175/JCLI-D-12-00579.1

Friedlingstein, P., Jones, M.W., O'Sullivan, M., Andrew, R.M., Hauck, J., Peters, G.P., Peters, W., Pongratz, J., Sitch, S., Le Quéré, C., Bakker, D.C.E., Canadell, J.G., Ciais, P., Jackson, R.B., Anthoni, P., Barbero, L., Bastos, A., Bastrikov, V., Becker, M., Bopp, L., Buitenhuis, E., Chandra, N., Chevallier, F., Chini, L.P., Currie, K.I., Feely, R.A., Gehlen, M., Gilfillan, D., Gkritzalis, T., Goll, D.S., Gruber, N., Gutekunst, S., Harris, I., Haverd, V., Houghton, R.A., Hurtt, G., Ilyina, T., Jain, A.K., Joetzjer, E., Kaplan, J.O., Kato, E., Klein Goldewijk, K., Korsbakken, J.I., Landschützer, P., Lauvset, S.K., Lefèvre, N., Lenton, A., Lienert, S., Lombardozzi, D., Marland, G., McGuire, P.C., Melton, J.R., Metzl, N., Munro, D.R., Nabel, J.E.M.S., Nakaoka, S.-I., Neill, C., Omar, A.M., Ono, T., Peregon, A., Pierrot, D., Poulter, B., Rehder, G., Resplandy, L., Robertson, E., Rödenbeck, C., Séférian, R., Schwinger, J., Smith, N., Tans, P.P., Tian, H., Tilbrook, B., Tubiello, F.N., van der Werf, G.R., Wiltshire, A.J., Zaehle, S., 2019. Global Carbon Budget 2019. Earth Syst. Sci. Data 11, 1783–1838. https://doi.org/10.5194/essd-11-1783-2019

Fung, I., Prentice, K., Matthews, E., Lerner, J., Russell, G., 1983. Three-dimensional tracer model study of atmospheric CO 2 : Response to seasonal exchanges with the terrestrial biosphere. J. Geophys. Res. 88, 1281. https://doi.org/10.1029/JC088iC02p01281

Gastellu-Etchegorry, J.P., 2008. 3D modeling of satellite spectral images, radiation budget and energy budget of urban landscapes. Meteorol. Atmos. Phys. 102, 187–207. https://doi.org/10.1007/s00703-008-0344-1

Goodrich, J.P., Campbell, D.I., Clearwater, M.J., Rutledge, S., Schipper, L.A., 2015. High vapor pressure deficit constrains GPP and the light response of NEE at a Southern

Hemisphere bog. Agric. For. Meteorol. 203, 54–63. https://doi.org/10.1016/j.agrformet.2015.01.001

Goudriaan, J., 1977. Crop Micrometeorology: a Simulation Study. Pudoc, Wageningen.

Hogan, R.J., Quaife, T., Braghiere, R., 2018. Fast matrix treatment of 3-D radiative transfer in vegetation canopies: SPARTACUS-Vegetation 1.1. Geosci. Model Dev. https://doi.org/10.5194/gmd-11-339-2018

Hogg, E.H., Barr, A.G., Black, T.A., 2013. A simple soil moisture index for representing multi-year drought impacts on aspen productivity in the western Canadian interior. Agric. For. Meteorol. 178–179, 173–182. https://doi.org/10.1016/j.agrformet.2013.04.025

Jacobs, C.M.J., 1994. Direct impact of atmospheric CO_2 enrichment on regional transpiration. PhD thesis, Wageningen Agricultural University, 1994.

Keenan, T.F., Prentice, I.C., Canadell, J.G., Williams, C., Wang, H., Raupach, M.R., Collatz, G.J., 2016. Recent pause in the growth rate of atmospheric CO2 due to enhanced terrestrial carbon uptake. Nat. Commun. https://doi.org/10.1038/ncomms13428

Kim, J., Guo, Q., Baldocchi, D., Leclerc, M., Xu, L., Schimid, H., 2006. Upscaling fluxes from tower to landscape: Overlaying flux footprints on high-resolution (IKONOS) images of vegetation cover. Agric. For. Meteorol. 136, 132–146. https://doi.org/10.1016/j.agrformet.2004.11.015

Kobayashi, H., Baldocchi, D.D., Ryu, Y., Chen, Q., Ma, S., Osuna, J.L., Ustin, S.L., 2012. Modeling energy and carbon fluxes in a heterogeneous oak woodland: A three-dimensional approach. Agric. For. Meteorol. 152, 83–100.

Kucharik, C.J., Norman, J.M., Gower, S.T., 1999. Characterization of radiation regimes in nonrandom forest canopies: theory, measurements, and a simplified modeling approach. Tree Physiol. 19, 695–706.

Le Quéré, C., Andrew, R.M., Friedlingstein, P., Sitch, S., Hauck, J., Pongratz, J., Pickers, P.A., Korsbakken, J.I., Peters, G.P., Canadell, J.G., Arneth, A., Arora, V.K., Barbero, L., Bastos, A., Bopp, L., Chevallier, F., Chini, L.P., Ciais, P., Doney, S.C., Gkritzalis, T., Goll, D.S., Harris, I., Haverd, V., Hoffman, F.M., Hoppema, M., Houghton, R.A., Hurtt, G., Ilyina, T., Jain, A.K., Johannessen, T., Jones, C.D., Kato, E., Keeling, R.F., Goldewijk, K.K., Landschützer, P., Lefèvre, N., Lienert, S., Liu, Z., Lombardozzi, D., Metzl, N., Munro, D.R., Nabel, J.E.M.S., Nakaoka, S., Neill, C., Olsen, A., Ono, T., Patra, P., Peregon, A., Peters, W., Peylin, P., Pfeil, B., Pierrot, D., Poulter, B., Rehder, G., Resplandy, L., Robertson, E., Rocher, M., Rödenbeck, C., Schuster, U., Schwinger, J., Séférian, R., Skjelvan, I., Steinhoff, T., Sutton, A., Tans, P.P., Tian, H., Tilbrook, B., Tubiello, F.N., van der Laan-Luijkx, I.T., van der Werf, G.R., Viovy, N., Walker, A.P., Wiltshire, A.J., Wright, R., Zaehle, S., Zheng, B., 2018. Global Carbon Budget 2018. Earth Syst. Sci. Data 10, 2141–2194. https://doi.org/10.5194/essd-10-2141-2018

Leblanc, S., Chen, J., Kwong, M., 2002. Tracing radiation and architecture of canopies. TRAC Manual. Version 2.1. 3. Nat. Resour. Canada, Canada Cent. 1–25.

Leblanc, S.G., Chen, J.M., Fernandes, R., Deering, D.W., Conley, A., 2005. Methodology comparison for canopy structure parameters extraction from digital hemispherical photography in boreal forests. Agric. For. Meteorol. 129, 187–207.

Li, X., Strahler, A.H., Woodcock, C.E., 1995. Hybrid geometric optical-radiative transfer approach for modeling albedo and directional reflectance of discontinuous canopies. IEEE Trans. Geosci. Remote Sens. 33, 466–480.

Loew, A., Van Bodegom, P.M., Widlowski, J.L., Otto, J., Quaife, T., Pinty, B., Raddatz, T., 2014. Do we (need to) care about canopy radiation schemes in DGVMs? Caveats and potential impacts. Biogeosciences 11, 1873–1897.

894 Loveland, T.R., Belward, A.S., 1997. The IGBP-DIS global 1km land cover data set,
895 DISCover: First results. Int. J. Remote Sens. 18, 3289–3295.
896 https://doi.org/10.1080/014311697217099
897 Ma, S., Baldocchi, D.D., Xu, L., Hehn, T., 2007. Inter-annual variability in carbon dioxide
898 exchange of an oak/grass savanna and open grassland in California. Agric. For. Meteorol.
899 147, 157–171.
900 Ma, S., Baldocchi, D., Wolf, S., Verfaillie, J., 2016. Slow ecosystem responses conditionally
901 regulate annual carbon balance over 15 years in Californian oak-grass savanna. Agric.
902 For. Meteorol. 228–229, 252–264. https://doi.org/10.1016/j.agrformet.2016.07.016
903 Mcmurtrie, R.E., Wang, Y.P., 1993. Mathematical-Models of the Photosynthetic Response of
904 Tree Stands to Rising Co2 Concentrations and Temperatures. Plant Cell Environ. 16, 1–
905 13.
906 Medlyn, B.E., Pepper, D.A., O'Grady, A.P., Keith, H., 2007. Linking leaf and tree water use
907 with an individual-tree model. Tree Physiol. 27, 1687–1699.
908 https://doi.org/10.1093/treephys/27.12.1687
909 Medlyn, B., 2004. A MAESTRO retrospective, in: Mencuccini, M., Grace, J., Moncrieff, J.B.,
910 McNaughton, K. (Eds.), Forests at the Land-Atmosphere Interface. CAB International,
911 pp. 105–121.
912 Mercado, L.M., Huntingford, C., Gash, J.H.C., Cox, P.M., Jogireddy, V., 2007. Improving the
913 representation of radiation interception and photosynthesis for climate model applications.
914 Tellus, Ser. B Chem. Phys. Meteorol. 59, 553–565. https://doi.org/10.1111/j.1600-
915 0889.2007.00256.x

916 Myneni, R.B., Ross, J., Asrar, G., 1989. A review on the theory of photon transport in leaf
917 canopies. Agric. For. Meteorol. 45, 1–153. https://doi.org/10.1016/0168-1923(89)90002-
918 6

Nelder, J. a., Mead, R., 1964. A simplex method for function minimization. Comput. J. 7, 308–313. https://doi.org/10.1093/comjnl/7.4.308

Ni, W., Li, X., Woodcock, C.E., Caetano, M.R., Strahler, A.H., 1999. An analytical hybrid GORT model for bidirectional reflectance over discontinuous plant canopies. IEEE Trans. Geosci. Remote Sens. 37, 987–999.

Nilson, T., 1971. A theoretical analysis of the frequency of gaps in plant stands. Agric. Meteorol. 8, 25–38. https://doi.org/10.1016/0002-1571(71)90092-6

Norman, J.M., Jarvis, P.G., 1974. Photosynthesis in Sitka spruce (Picea sitchensis (Bong.) Carr.). III. Measurements of canopy structure and interception of radiation. J. Appl. Ecol. https://doi.org/10.2307/2402028

Norman, J.M.M., 1979. Modeling the complete crop canopy, in: Barfield, B., Gerber, J. (Eds.), Modification of the Aerial Environment of Plants. Am. Soc. Agric. Eng. Monogr. No. 2, ASAE, pp. 249–277.

Norman, J., Welles, J., 1983. Radiative transfer in an array of canopies. Agron. J. 75, 481–488.

Norman, J.M., 1993. Scaling Processes between Leaf and Canopy Levels, in: Scaling Physiological Processes: Leaf to Globe. https://doi.org/10.1016/B978-0-12-233440-5.50010-5

Norton, A.J., Rayner, P.J., Koffi, E.N., Scholze, M., Silver, J.D., Wang, Y.-P., 2019. Estimating global gross primary productivity using chlorophyll fluorescence and a data assimilation system with the BETHY-SCOPE model. Biogeosciences 16, 3069–3093. https://doi.org/10.5194/bg-16-3069-2019

Oleson, K.W., Lawrence, D.M., Gordon, B., Flanner, M.G., Kluzek, E., Peter, J., Levis, S., Swenson, S.C., Thornton, E., Feddema, J., 2010. Technical description of version 4.0 of the Community Land Model (CLM). NCAR/TN-478+STR NCAR Tech. Note. https://doi.org/10.5065/D6RR1W7M

Osuna, J.L., Baldocchi, D.D., Kobayashi, H., Dawson, T.E., 2015. Seasonal trends in photosynthesis and electron transport during the Mediterranean summer drought in leaves of deciduous oaks. Tree Physiol. https://doi.org/10.1093/treephys/tpv023

Otsu, N., 1979. Threshold selection method from grey-level histograms. IEEE Trans Syst Man Cybern. https://doi.org/10.1109/TSMC.1979.4310076

Pinty, B., 2004. Radiation Transfer Model Intercomparison (RAMI) exercise: Results from the second phase. J. Geophys. Res. 109, D06210. https://doi.org/10.1029/2003JD004252

Pinty, B., Lavergne, T., Dickinson, R.E., Widlowski, J.L., Gobron, N., Verstraete, M.M., 2006. Simplifying the interaction of land surfaces with radiation for relating remote sensing products to climate models. J. Geophys. Res. Atmos. 111.

Pitman, A.J., 2003. The evolution of, and revolution in, land surface schemes designed for climate models. Int. J. Climatol. https://doi.org/10.1002/joc.893

Prentice, I.C., Liang, X., Medlyn, B.E., Wang, Y.P., 2015. Reliable, robust and realistic: The three R's of next-generation land-surface modelling. Atmos. Chem. Phys. https://doi.org/10.5194/acp-15-5987-2015

Raz-Yaseef, N., Koteen, L., Baldocchi, D.D., 2013. Coarse root distribution of a semi-arid oak savanna estimated with ground penetrating radar. J. Geophys. Res. Biogeosciences 118, 135–147. https://doi.org/10.1029/2012JG002160

Rich, P.M., Chen, J., Sulatycki, S.J., Vashisht, R., Wachspress, W.S., 1995. Calculation of leaf area index and other canopy indices from gap fraction: a manual for the LAICAL software.

Rich, P.M., Fournier, R.A., 1999. Data, BOREAS TE-23 Map Plot. https://doi.org/http://dx.doi.org/10.3334/ORNLDAAC/359

Rich, P.M., 1990. Characterizing plant canopies with hemispherical photographs. Remote Sens. Rev. 5, 13–29. https://doi.org/10.1080/02757259009532119

969 Rich, P.M., 1989. A Manual for Analysis of Hemispherical Canopy Photography., Science.
970 Ross, J., 1981. The radiation regime and architecture of plant stands. Junk, Boston.
971 https://doi.org/10.1007/978-94-009-8647-3
972 Ryu, Y., Nilson, T., Kobayashi, H., Sonnentag, O., Law, B.E., Baldocchi, D.D., 2010. On the
973 correct estimation of effective leaf area index: Does it reveal information on clumping
974 effects? Agric. For. Meteorol. 150, 463–472.
975 Ryu, Y., Sonnentag, O., Nilson, T., Vargas, R., Kobayashi, H., Wenk, R., Baldocchi, D.D.,
976 2010. How to quantify tree leaf area index in an open savanna ecosystem: A multi-
977 instrument and multi-model approach. Agric. For. Meteorol. 150, 63–76.
978 https://doi.org/10.1016/j.agrformet.2009.08.007
979 Schaefer, K., Schwalm, C.R., Williams, C., Arain, M.A., Barr, A., Chen, J.M., Davis, K.J.,
980 Dimitrov, D., Hilton, T.W., Hollinger, D.Y., Humphreys, E., Poulter, B., Raczka, B.M.,
981 Richardson, A.D., Sahoo, A., Thornton, P., Vargas, R., Verbeeck, H., Anderson, R.,
982 Baker, I., Black, T.A., Bolstad, P., Chen, J., Curtis, P.S., Desai, A.R., Dietze, M., Dragoni,
983 D., Gough, C., Grant, R.F., Gu, L., Jain, A., Kucharik, C., Law, B., Liu, S., Lokipitiya, E.,
984 Margolis, H.A., Matamala, R., McCaughey, J.H., Monson, R., Munger, J.W., Oechel, W.,
985 Peng, C., Price, D.T., Ricciuto, D., Riley, W.J., Roulet, N., Tian, H., Tonitto, C., Torn,
986 M., Weng, E., Zhou, X., 2012. A model-data comparison of gross primary productivity:
987 Results from the North American Carbon Program site synthesis. J. Geophys. Res.
988 Biogeosciences 117, n/a-n/a. https://doi.org/10.1029/2012JG001960
989 Schwarz, G., 1978. Estimating the Dimension of a Model. Ann. Stat. 6, 461–464.
990 https://doi.org/10.1214/aos/1176344136
991 Sellers, P.J., 1985. Canopy reflectance, photosynthesis and transpiration. Int. J. Remote Sens.
992 6, 1335–1372. https://doi.org/10.1080/01431168508948283

Sellers, P.J., Randall, D.A., Collatz, G.J., Berry, J.A., Field, C.B., Dazlich, D.A., Zhang, C., Collelo, G.D., Bounoua, L., 1996. A Revised Land Surface Parameterization (SiB2) for Atmospheric GCMS. Part I: Model Formulation. J. Clim. 9, 676–705. https://doi.org/10.1175/1520-0442(1996)009<0676:ARLSPF>2.0.CO;2

Sellers, P.J., 1997. Modeling the Exchanges of Energy, Water, and Carbon Between Continents and the Atmosphere. Science (80-.). 275, 502–509. https://doi.org/10.1126/science.275.5299.502

Song, C., Katul, G., Oren, R., Band, L.E., Tague, C.L., Stoy, P.C., McCarthy, H.R., 2009. Energy, water, and carbon fluxes in a loblolly pine stand: Results from uniform and gappy canopy models with comparisons to eddy flux data. J. Geophys. Res. Biogeosciences 114, 1–18. https://doi.org/10.1029/2009JG000951

Spencer, S., Rock, B.N., 1999. BOREAS TE-08 Aspen Bark Spectral Reflectance Data. https://doi.org/10.3334/ORNLDAAC/336

Thornton, P.E., Zimmermann, N.E., 2007. An Improved Canopy Integration Scheme for a Land Surface Model with Prognostic Canopy Structure. J. Clim. 20, 3902–3923. https://doi.org/10.1175/JCLI4222.1

Vezy, R., Christina, M., Roupsard, O., Nouvellon, Y., Duursma, R., Medlyn, B., Soma, M., Charbonnier, F., Blitz-Frayret, C., Stape, J.-L., Laclau, J.-P., de Melo Virginio Filho, E., Bonnefond, J.-M., Rapidel, B., Do, F.C., Rocheteau, A., Picart, D., Borgonovo, C., Loustau, D., le Maire, G., 2018. Measuring and modelling energy partitioning in canopies of varying complexity using MAESPA model. Agric. For. Meteorol. 253–254, 203–217. https://doi.org/10.1016/j.agrformet.2018.02.005

Walter, J.-M., 2012. CIMES-FISHEYE © 2009–2015 HEMISPHERICAL PHOTOGRAPHY OF FOREST CANOPIES.

Walters, D.N., Williams, K.D., Boutle, I.A., Bushell, A.C., Edwards, J.M., Field, P.R., Lock, A.P., Morcrette, C.J., Stratton, R.A., Wilkinson, J.M., Willett, M.R., Bellouin, N., Bodas-Salcedo, A., Brooks, M.E., Copsey, D., Earnshaw, P.D., Hardiman, S.C., Harris, C.M., Levine, R.C., Maclachlan, C., Manners, J.C., Martin, G.M., Milton, S.F., Palmer, M.D., Roberts, M.J., Rodríguez, J.M., Tennant, W.J., Vidale, P.L., 2014. The Met Office Unified Model Global Atmosphere 4.0 and JULES Global Land 4.0 configurations. Geosci. Model Dev. 7, 361–386.

Wang, Y.P., Jarvis, P.G., 1990. Influence of crown structural properties on PAR absorption, photosynthesis, and transpiration in Sitka spruce: application of a model (MAESTRO). Tree Physiol. 7, 297–316. https://doi.org/10.1093/treephys/7.1-2-3-4.297

Wang, Y.P., Rey, A., Jarvis, P.G., 1998. Carbon balance of young birch trees grown in ambient and elevated atmospheric CO2 concentrations. Glob. Chang. Biol. 4, 797–807.

Wang, Y.P., Jarvis, P.G., 1990. Description and validation of an array model — MAESTRO. Agric. For. Meteorol. https://doi.org/10.1016/0168-1923(90)90112-J

Wang, W.M., Li, Z.L., Su, H.B., 2007. Comparison of leaf angle distribution functions: Effects on extinction coefficient and fraction of sunlit foliage. Agric. For. Meteorol. 143, 106–122. https://doi.org/10.1016/j.agrformet.2006.12.003

Widlowski, J.L., Pinty, B., Clerici, M., Dai, Y., De Kauwe, M., De Ridder, K., Kallel, A., Kobayashi, H., Lavergne, T., Ni-Meister, W., Olchev, A., Quaife, T., Wang, S., Yang, W., Yang, Y., Yuan, H., 2011. RAMI4PILPS: An intercomparison of formulations for the partitioning of solar radiation in land surface models. J. Geophys. Res. G Biogeosciences 116.

Wieder, W.R., Cleveland, C.C., Smith, W.K., Todd-Brown, K., 2015. Future productivity and carbon storage limited by terrestrial nutrient availability. Nat. Geosci. 8, 441–444. https://doi.org/10.1038/ngeo2413

Williams, K., Gornall, J., Harper, A., Wiltshire, A., Hemming, D., Quaife, T., Arkebauer, T., Scoby, D., 2017. Evaluation of JULES-crop performance against site observations of irrigated maize from Mead, Nebraska. Geosci. Model Dev. 10, 1291–1320. https://doi.org/10.5194/gmd-10-1291-2017

Xu, L., Baldocchi, D.D., 2003. Seasonal trends in photosynthetic parameters and stomatal conductance of blue oak (Quercus douglasii) under prolonged summer drought and high temperature. Tree Physiol. https://doi.org/10.1093/treephys/23.13.865

Yang, W., Ni-Meister, W., Kiang, N.Y., Moorcroft, P.R., Strahler, A.H., Oliphant, A., 2010. A clumped-foliage canopy radiative transfer model for a Global Dynamic Terrestrial Ecosystem Model II: Comparison to measurements. Agric. For. Meteorol. 150, 895–907. https://doi.org/10.1016/j.agrformet.2010.02.008

Zhang, Y., Song, C., Band, L.E., Sun, G., 2019. No Proportional Increase of Terrestrial Gross Carbon Sequestration From the Greening Earth. J. Geophys. Res. Biogeosciences 2018JG004917. https://doi.org/10.1029/2018JG004917

Zhu, Z., Piao, S., Myneni, R.B., Huang, M., Zeng, Z., Canadell, J.G., Ciais, P., Sitch, S., Friedlingstein, P., Arneth, A., Liu, R., Mao, J., Pan, Y., Peng, S., Peñuelas, J., Poulter, B., 2016. Greening of the Earth and its drivers. Nat. Clim. Chang. https://doi.org/10.1038/NCLIMATE3004

1064 a. b.

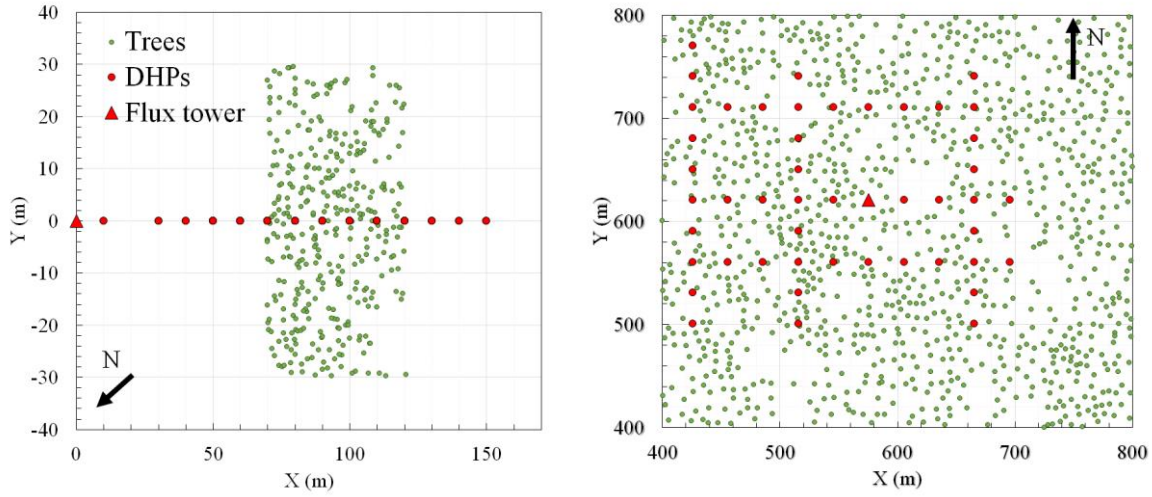

1065

1066 c. d.

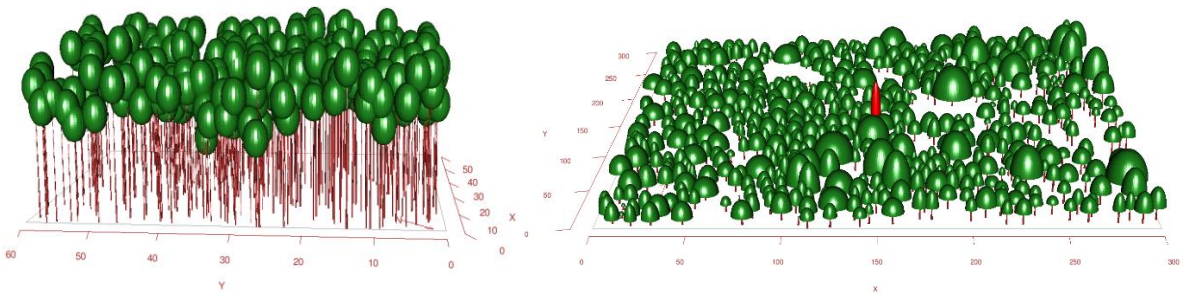

1067

1068 e. f.

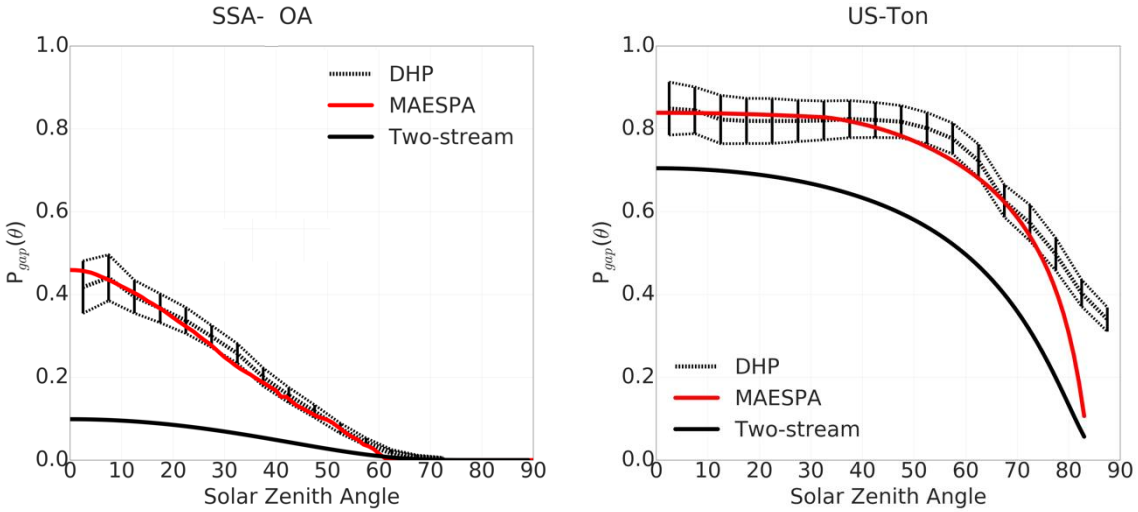

1069

1070 Figure 1: Map plot of (a.) an old aspen site in Canada (SSA-OA: 53.88° N,104.65° W), and

1071 (b.) blue oak grassland in California, USA (US-Ton: 38.43° N, 120.97° W); 3D representation

of forest canopies in MAESPA created with the R package Maeswrap for (c.) SSA-OA an(d.) US-Ton. The red element in the centre of Figure 1.0d represents the flux tower; and direct transmittance zenith profile calculated with the MAESPA model, the two-stream scheme, and measured through DHPs for (e.) SSA-OA and (f.) US-Ton. The vertical bars represent the 95% CI of the mean.

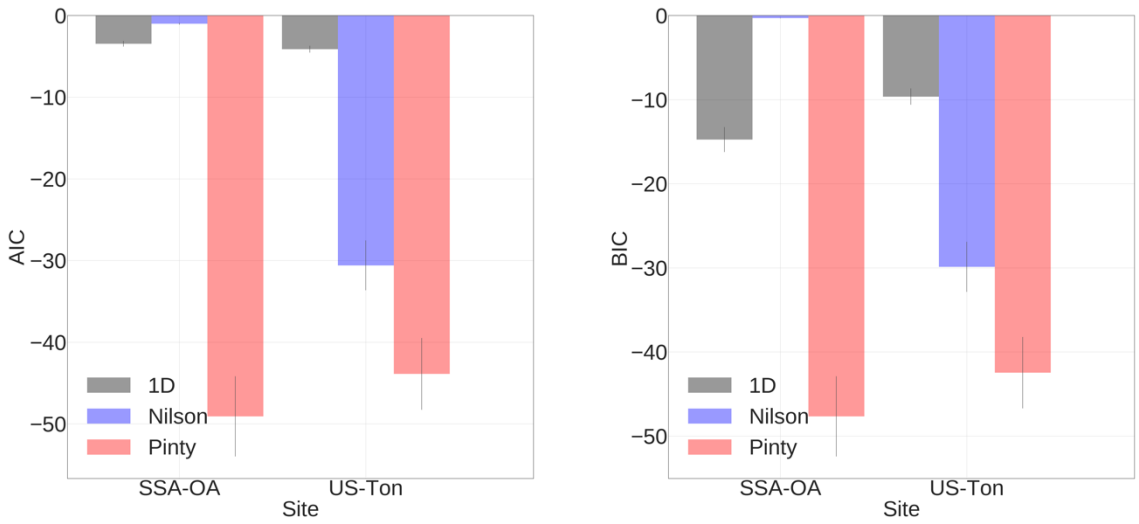

Figure 2: Comparison of (a.) RMSE and (b.) AIC between Beer's law (1D), clumping index (Nilson), and structure factor (Pinty) for SSA-OA and US-Ton.

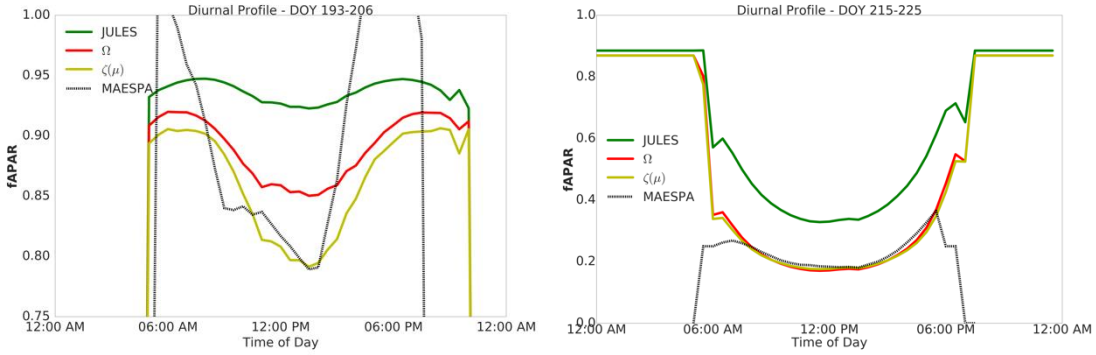

(a) SSA – OA (b) US – Ton

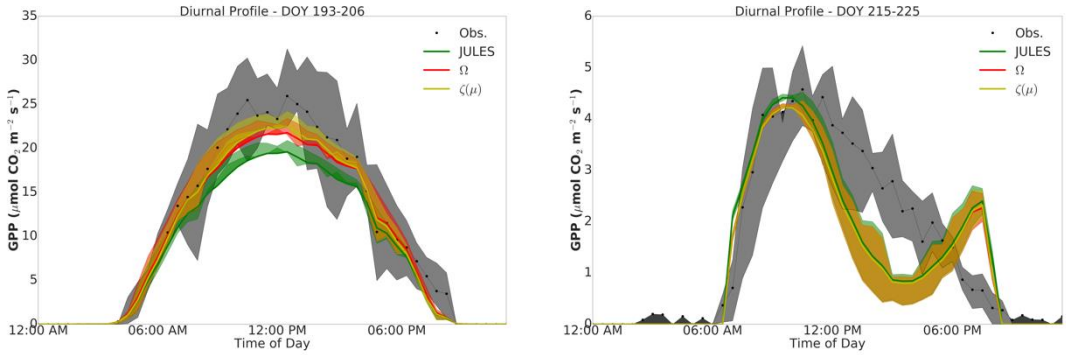

(c) SSA – OA (d) US – Ton

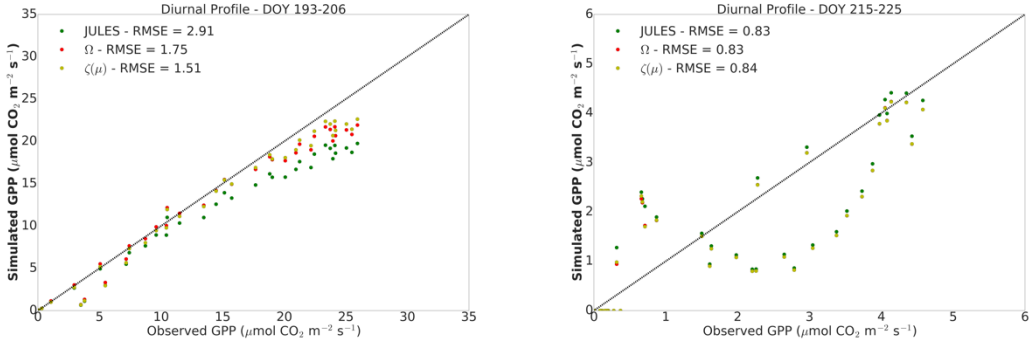

(e) SSA – OA (f) US – Ton

Figure 3: (a.) and (b.) fAPAR; (c.) and (d.) GPP vs. local time; and (e.) and (f.) modeled and flux tower GPP correlation for an old aspen site in Canada (SSA-OA) and a blue oak savannah site in California (US-Ton), respectively. The shaded areas represent the 25 % and 75% quartiles of the average.

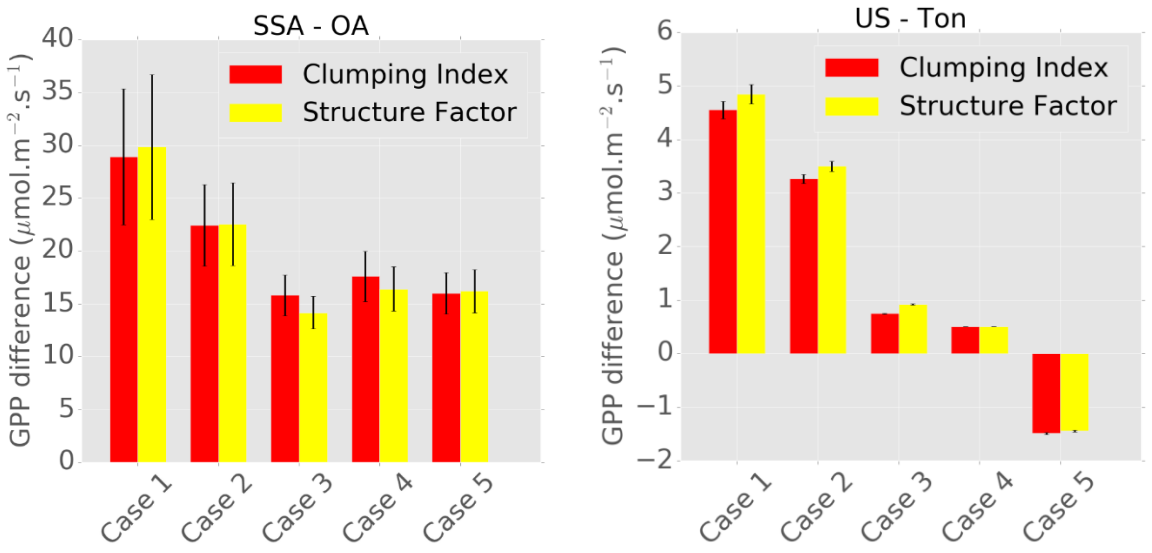

Figure 4: Integrated difference in GPP between the modified JULES with both clumping indices, clumping index and structure factor, and the default non-clumped version summed across 10 vertical layers and throughout the Sun zenith angular interval for (a.) SSA-OA and (b.) US-Ton. Associated deviations are shown as black error bars and represent the mean squared deviation (MSD).

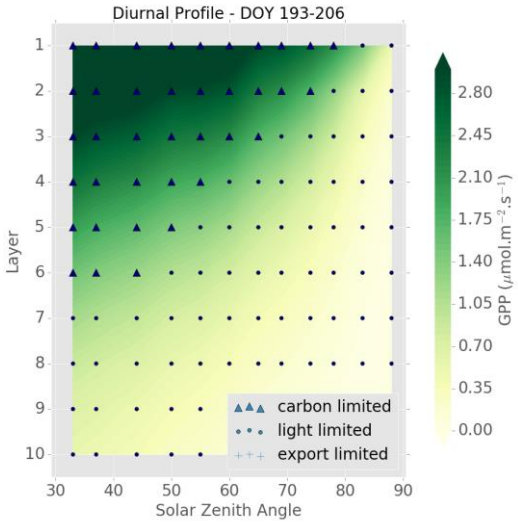

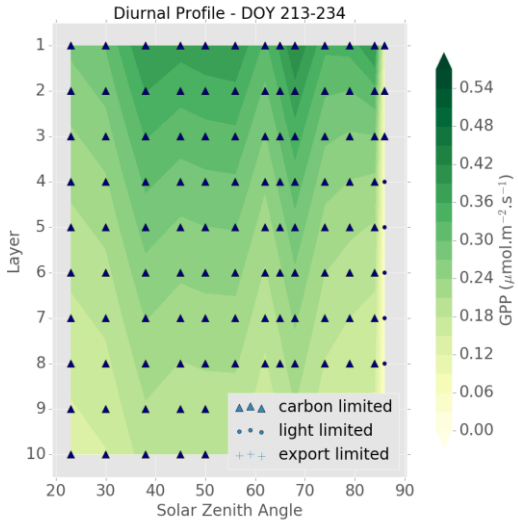

1119

1120 (a) SSA – OA (b) US – Ton

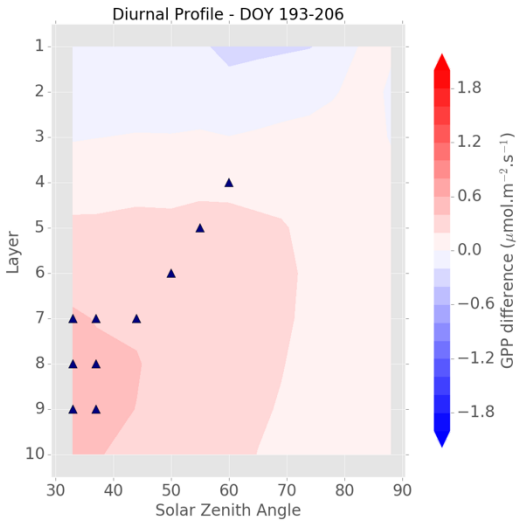

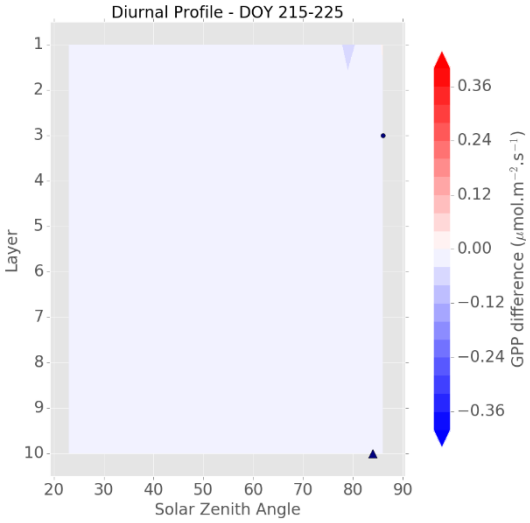

1121

1122 (c) SSA – OA (d) US – Ton

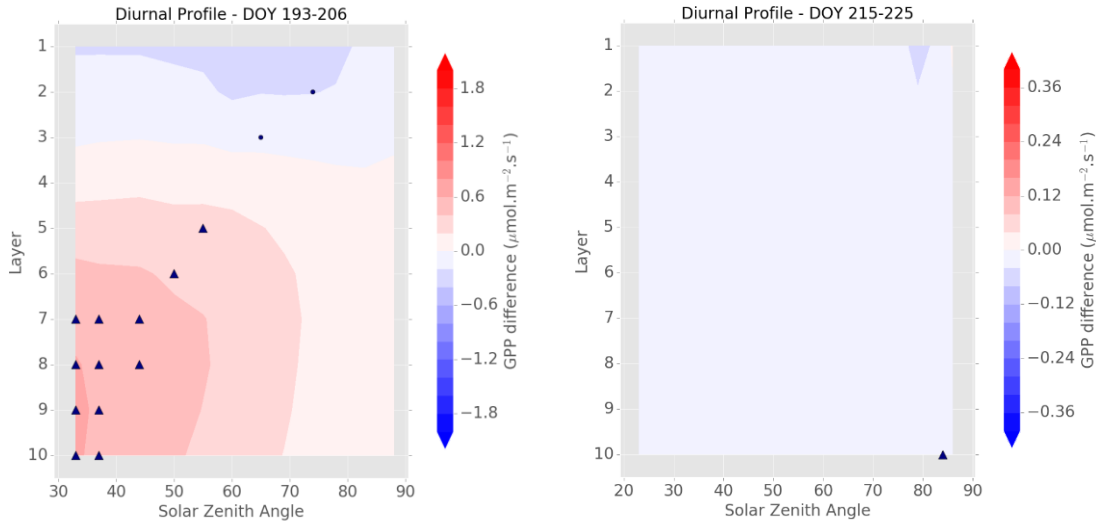

1123

1124 (e) SSA – OA (f) US – Ton

1125 Figure 5: (a.) and (b.) vertical zenith profile of photosynthesis limiting regimes in JULES; (c.)
1126 and (d.) GPP difference between the modified two-stream with clumping index (Ω) minus the
1127 non-clump version; and (e.) and (f.) GPP difference between the modified two-stream with
1128 structure factor (ζ(μ)) minus the non-clump version. Symbols represented in figures from (c.)
1129 to (f.) indicate difference in photosynthesis limiting between model set ups, i.e., carbon (▲),
1130 light (●), and electron export (+).

Table 1: Study sites categorized by plant functional type (PFT)*, country, latitude and longitude, climate, and dominant tree species. P_{gap} column indicates the derivation method: DHP for digital hemispherical photographs; and 3D refers to the 3D tree-based model MAESPA.

PFT	COUNTRY	SITE	LATITUDE	LONGITUDE	CLIMATE	DOMINANT SPECIES	$P_{GAP}(\Theta)$
DBF	Canada	SSA-OA	53.876	104.645	Boreal	Aspen	DHP & 3D modeling
WSA	USA	US-Ton	38.432	120.966	Mediterranean	Blue Oak	DHP & 3D modeling

* DBF: Deciduous Broadleaf Forest; WSA: Woody-Savannah.

Table 2: Summary of statistical evaluations for both study sites including AIC, BIC, R, and RMSE.

STUDY SITE	LAI ($M.M^{-2}$)	TREE DENSITY ($TREES.HA^{-1}$)	INDEX	VALUE (95% CI)	AIC	BIC	R	RMSE
SSA-OA	4.63	1068	Ω	0.660(0.585,0.734)	-1.07	-0.31	0.977	0.116
			ζ(μ)	a = 0.394(0.356,0.432); b = 0.627(0.517,0.736)	-49.09	-47.67	0.997	0.016
US-TON	0.70	144	Ω	0.462(0.434,0.490)	-30.60	-29.89	0.958	0.022
			ζ(μ)	a = 0.492(0.447,0.537); b^{*} = -0.097(-0.230,0.031)	-43.89	-42.47	0.960	0.023

*p-value = 0.123. All other p-values < 0.

1142 Table 3: Five different model setups to evaluate the impact of structural parameterization schemes on JULES GPP and their interactions with other
1143 factors affecting photosynthesis performed for both study sites, i.e., an old aspen site in Canada (SSA-OA) and a blue oak savannah site in
1144 California (US-Ton), with results presented in Figure 4.

1145

Case	Description	Reference integrated vertical GPP ($\mu molCO_2 m^{-2} s^{-1}$) summed over all SZA from JULES for SSA - OA	Reference integrated vertical GPP ($\mu molCO_2 m^{-2} s^{-1}$) summed over all SZA from JULES for US - Ton
1	All incident shortwave radiation is direct, soil reflectance is zero, leaf reflectance and transmittance are zero, and the vertical profile of leaf nitrogen concentration is constant and equal to the top leaf nitrogen concentration in kg N $[kg\ C]^{-1}$.	82.18	26.67

2	All incident shortwave radiation is direct, soil reflectance is zero, leaf reflectance and transmittance are zero, and the vertical profile of leaf nitrogen concentration varies with canopy layers.	72.70	20.39
3	All incident shortwave radiation is direct, soil reflectance is zero, leaf reflectance and transmittance are set to measured values, and the vertical profile of leaf nitrogen concentration varies with canopy layers.	99.52	23.88
4	All incident shortwave radiation is direct, soil reflectance is set to a measured value, leaf reflectance	100.93	26.38

	and transmittance are set to measured values, and the vertical profile of leaf nitrogen concentration varies with canopy layers.		
5	All incident shortwave radiation is given in terms of direct and diffuse proportions from measurements, soil reflectance is set to a measured value, leaf reflectance and transmittance are set to measured values, and the vertical profile of leaf nitrogen concentration varies with canopy layers.	135.64	29.84

1146

Supplementary material and Additional information

Appendix A: Modified two-stream scheme

The modified two-stream equations described in this section make use of the clumping index of Pinty et al. (2006), the so-called structure factor ζ(μ); however, the addition of the other clumping index is analogous to the structure factor by not considering sun angular variations on the structure factor, i.e., making b = 0 in Eq. 4.0.

The structure factor can be included on the optical depth of direct beam per unit leaf area, by modifying K as:

$$K_\zeta = \frac{G(\theta)}{\mu} \cdot \zeta(\mu) \quad \text{(A1.0)}$$

The same analogy can be applied when calculating the average inverse diffuse optical depth per unit leaf area, $\bar{\mu}$, but obtaining the structure factor for the direction of scattered flux, μ':

$$\bar{\mu_\zeta} = \int_0^1 \frac{\mu'}{G(\mu')\cdot\zeta(\mu')}\, d\mu' \quad \text{(A2.0)}$$

The parameter ωβ can be inferred from the analysis of Norman and Jarvis (1975) in the case of a single leaf whose normal is oriented at zenith angle θ_l from the local vertical defined in the upward hemisphere (Pinty et al., 2006):

$$\omega\beta = \frac{1}{2}(\omega + \delta_l \cos^2\theta_l) \quad \text{(A3.0)}$$

Where $\omega = \rho_{leaf} + \rho_{leaf}$ and $\delta_l = \rho_{leaf} - \rho_{leaf}$. Eq. 6 is only valid for a single leaf, and in order to obtain the total contribution of leaves over the canopy, it is necessary to integrate it over the appropriate leaf orientation probability distribution, i.e., between 0 and π/2, because the leaf normal is assumed to be oriented into the upward hemisphere. And when isolating β, it is possible to obtain the generic diffuse upscatter parameter:

$$\beta = \frac{1}{2\omega}\left(\omega + \delta_l \int_0^{\pi/2} \cos^2\theta_l\, g'(\theta_l) \sin\theta_l\, d\theta_l\right) \quad \text{(A4.0)}$$

where sin θ_l is introduced for normalisation requirement of the probability distribution function. If the two-stream scheme equations are solved when $\omega \rightarrow 0$, i.e., single scatter approximation and semi-infinite canopy, the upward diffuse flux at the top of the canopy may be taken as equal to the single scattering albedo ($a_s(\mu)$). The equation for the direct upscatter parameter, β_0, is

$$\beta = \frac{1+\bar{\mu}K}{\omega\bar{\mu}K}\alpha_s(\mu) \quad \text{(A5.0)}$$

And ($a_s(\mu)$) is given by,

$$\alpha_s(\mu) = \frac{\omega}{2}\int_0^1 \frac{\mu' G(\mu)}{\mu G(\mu')\cdot\mu' G(\mu)} d\mu' \quad \text{(A6.0)}$$

The equation above is only valid when assuming isotropic scattering for the leaf elements, which makes the scattering phase function independent of the angle of the incident beam (Dickinson, 1983; Sellers, 1985).

The addition of the structure factor into the single scattering albedo formulation results in,

$$\alpha_s(\mu) = \frac{\omega}{2}\int_0^1 \frac{\mu' G(\mu)\zeta(\mu)}{\mu G(\mu')\zeta(\mu') + \mu' G(\mu)\zeta(\mu)} d\mu' \quad \text{(A7.0)}$$

In this case the formulation for the direct upscatter parameter considering canopy structure is:

$$\beta_0 = \frac{1+\bar{\mu}_\zeta K_\zeta}{\omega\bar{\mu}_\zeta K_\zeta}\left[\frac{\omega}{2}\int_0^1 \frac{\mu' G(\mu)\zeta(\mu)}{\mu G(\mu')\zeta(\mu') + \mu' G(\mu)\zeta(\mu)} d\mu'\right] \quad \text{(A8.0)}$$

The new variables K_ζ, $\bar{\mu}_\zeta$, and the modified upscattering parameters for the diffuse and direct beams, β and β_0, are applied into Eq. 3.0 to modify the two-stream scheme.

Appendix B: DHPs pre-processing

The P_{gap} zenith curve from each DHP is represented in Figure A.1 by a coloured line and the average is represented by the central thick black line with the 95% confidence interval of the mean represented by vertical bars.

Note that overall sites with higher LAI present lower values of direct transmittance because LAI is one of the major factors controlling the shape of the P_{gap} zenith curves but not the only one, therefore study sites with same LAI can present distinct direct transmittance zenith profiles.

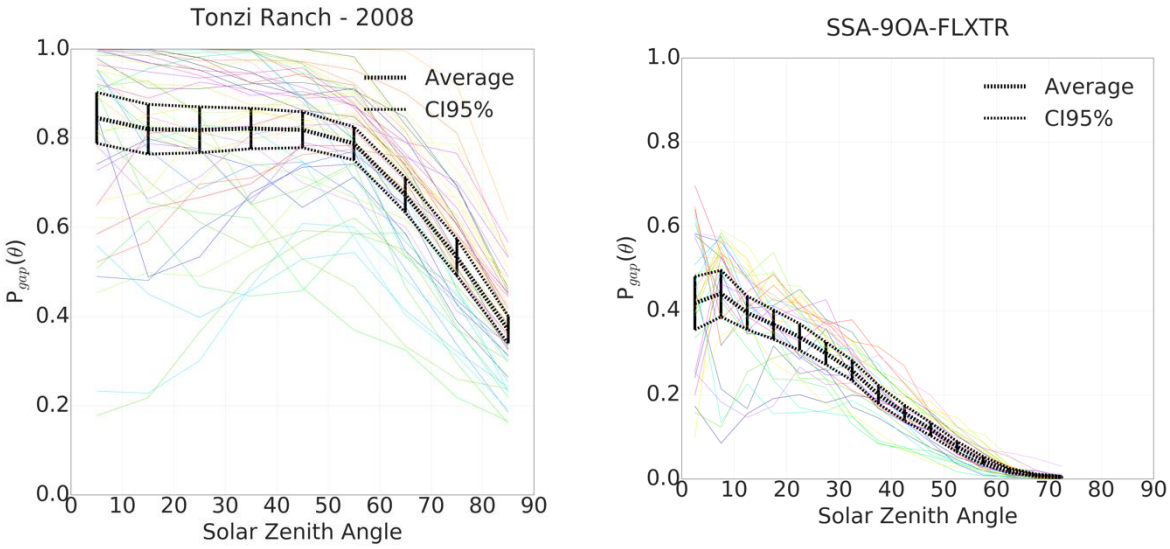

(a) LAI = 0.70 $m^2.m^{-2}$ (b) LAI = 4.63 $m^2.m^{-2}$

Figure A.1: $P_{gap}(\theta)$ derived from DHPs for 2 study sites described in Table 1. Colored lines represent individual DHPs and the black line represents the mean. Vertical bars represent the 95% CI of the mean.

Appendix C: Example of derivation of clumping indices from observed data

An example of fitting is shown in Figure A.2 for the same two sites evaluated before, but the same evaluation was performed for all the other sites and the results are summarised in Table 2.0. The LAI for both sites was estimated from different sources that not DHPs in order to avoid circularity, as previously mentioned. For the old aspen site, the LAI was obtained through LAI-2000, while for the blue oak savannah site the LAI was obtained from multiple sources described in Ryu et al. (2010).

The parameters were isolated through two different methodologies:

1. to obtain the clumping index from Nilson (1971) Eq. 3.0 was inverted as:

$$-\ln\left(P_{gap}\right)\cdot G(\mu)^{-1}\cdot LAI^{-1}=\Omega\cdot\frac{1}{\mu} \quad \text{(C1.0)}$$

A linear fit with one free parameter, i.e., with the line forced to cross zero against 15 data points of direct transmittance obtained from DHPs. Aho et al. (2014) found that for ecological publications from 1993 to 2013, the two most popular measures of model's parsimony were the Akaike information criterion (AIC; Akaike (1973)) and the Bayesian information criterion (BIC; Schwarz (1978)). The AIC and BIC are statistical variables that represent how accurately a model fits the data, and the lower their values are, the better the evaluated model. The correlation coefficient (r), RMSE, AIC, and BIC were calculated for the fit and are presented in Figure A.2a for two sites.

2. to obtain the structure factor parameters from Pinty et al. (2006) Eq. 3.0 with (Ω(θ)) given by Eq. 4.0 was inverted as:

$$-\ln\left(P_{gap}\right)\cdot\mu\cdot G(\mu)^{-1}\cdot LAI^{-1}=a+b\cdot(1-\mu) \quad \text{(C2.0)}$$

A linear fit with two free parameters was then adjusted against the same 15 data points of direct transmittance obtained through DHPs. The correlation coefficient, RMSE, AIC, and BIC were also calculated for the second fit.

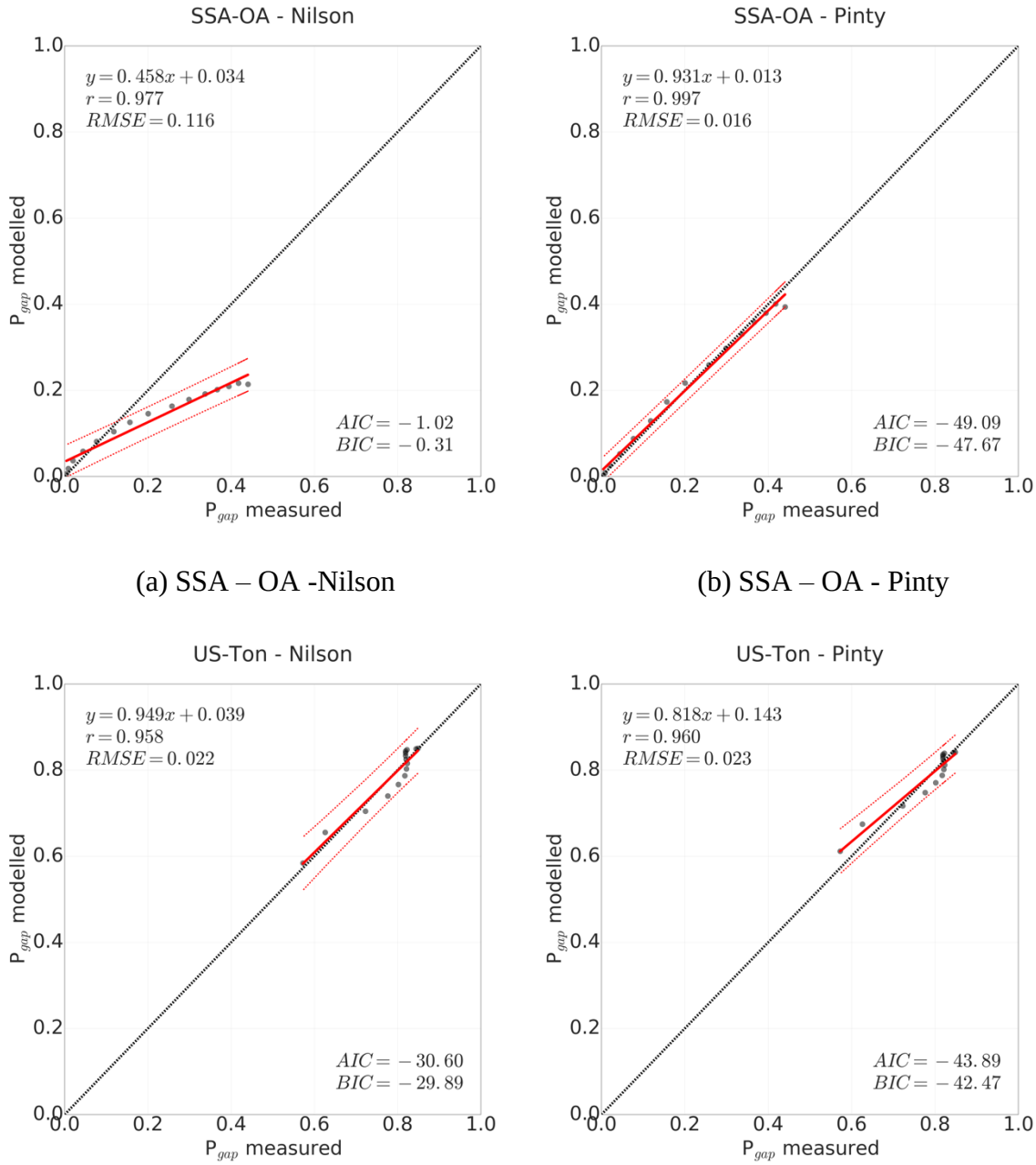

(a) SSA – OA -Nilson (b) SSA – OA - Pinty

(c) US – Ton -Nilson (d) US – Ton - Pinty

Figure A.2: Old aspen site in Canada (SSA-OA: 53.88 N,104.65 W) with LAI = 4.63 $m^2.m^{-2}$ for (a.) clumping index (Ω) from Nilson (1971), and (b.) structure factor (ζ(μ)) from Pinty et al. (2006); and blue oak savannah in California, USA (US-Ton: 38.43 N, 120.97 W) with LAI = 0.70 $m^2.m^{-2}$ for (c.) clumping index (Ω), and (d.) structure factor (ζ(μ)).

Appendix D: Mean squared deviation (MSD)

The associated deviations for each scenario described in Section 4.4.1 were calculated following the mean squared deviation (MSD):

$$MSD = \frac{1}{n \cdot nSZA} \sum_{i=1}^{n} \sum_{\theta=0°}^{SZA} \left| GPP_{clump}(i,\theta) - GPP_{non-clump}(i,\theta) \right|^2 \quad \text{(D1.0)}$$

where n is the number of canopy layers, i.e., n = 10, nSZA is the number of sun zenith angle intervals used in the experiment, i.e., nSZA = 15, and SZA is the maximum sun zenith angle (90°). GPP_{clump} is GPP calculated by JULES with each one of the two parameterization schemes, i.e., clumping index and structure factor, and $GPP_{non\text{-}clump}$ is GPP calculated by the original version of JULES.

1252